DEGREE PROJECT IN MATERIALS DESIGN AND ENGINEERING, SECOND CYCLE, 30 CREDITS

STOCKHOLM, SWEDEN 2018

Optimizing the slag system for phosphorus removal in a DRI-based EAF-process using the dictionary attack method

JOAR HUSS

KTH ROYAL INSTITUTE OF TECHNOLOGY
SCHOOL OF INDUSTRIAL ENGINEERING AND MANAGEMENT

“It may seem as if the mind is at its creative optimum, ever looking for solutions, when the stakes are high and the constraints imposed limitless. Whether these conditions arise from war, famine or sickness one thing is sure, the destruction of this planet might give rise to all this and possibly more, should mankind fail to meet this task. The carbon emissions produced by the steel industry must be lowered and it will require all the ingenuity we can muster. Great innovations are born out of great necessity.”

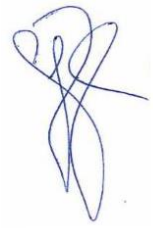

Joar Huss
Bergsingenjör

Table of Contents

Abstract

Carbon emissions pose a serious threat to the continued survival of this planet. All sectors of society must, therefore, lower their emissions, this includes the steel industry. The production of steel is based on iron ore reduction by carbon. In an attempt to relieve the steel industry from its inherent fossil dependence an initiative called HYBRIT has been started. It aims to supplant carbon reduction with hydrogen reduction. Currently, there is no economically viable industrial production of steel that uses fossil-free hydrogen as reduction agent. In order to create economic viability for such a process work has to be conducted to innovate and optimize. This study aims to be a part of that optimization process by creating a tool for optimizing the slag system with regards to phosphorus removal.

26843 slag compositions were evaluated using modules written in “Matlab” combined with “Thermo-Calc”. 1583 possible slag compositions were found to be suitable for phosphorus removal. These compositions were then optimized after slag weight in order to minimize slag associated cost. The compositions were tested against two theoretical raw materials with varying initial phosphorus content 250 ppm and 125 ppm. It was found that the initial phosphorus concentration of the raw material has a substantial impact not only on the slag costs but also the slag praxis that should be used.

1. Introduction

Carbon dioxide, a word that is heard every day. News channels, radio programs, blogs, podcasts and UN-reports all talking, informing, trying to convey that this is the stuff of nightmares. Sometimes their message falls on deaf ears and that wouldn't be such a problem if not only world leaders and industry directors were among those requiring hearing aid, but not always. Sometimes the message is heard loud and clear. Recently SSAB, LKAB and Vattenfall announced a joint venture, to stop carbon emissions associated with the production of steel, called HYBRIT (1) (2) (3). The initiators aim to make the blast furnace process route obsolete by creating economic viability in the electric arc furnace route using iron, which is direct reduced by hydrogen, as raw material. This way the main product of the steel industry will seize being carbon dioxide, after all, today two tons of carbon emission are created for every ton of steel produced (4).

To create economic viability, the initiative needs to innovate, question pre-existing biases, challenge established process praxis, think creatively and optimize each and every process step, to do more with less. Some claim that this initiative has the potential of reducing carbon emissions in Sweden by 10% (3). This might not sound like much, yet, if hydrogen reduced iron would be adopted on a global scale the impact will surely be significant.

1.1. Aim of work

According to the prefeasibility study, released in 2018, the HYBRIT enterprise is technologically possible, yet, it will come at a cost as the premium of a DRI-based steel would be 20-30% to maintain existing margins (5). To create a viable business model this gap must be closed. European allowance rights (EUAs) price is expected to rise (5) which will help narrow the gap, however, more must be done. Work towards optimization of the shaft furnace and the EAF will be important contributors in closing the gap. This work aims to harmonize the slag system in the EAF-process with DRI of different grades by cost optimization with regards to phosphorus removal.

2. Background

Iron has been used since the ancient Egyptians discovered metallic iron in meteors and was regarded as a material of kings (6) (7). Today mankind no longer needs to rely on meteors to strike the earth, instead we have learned to harvest iron from its crust. In its pure form it has a greyish metallic tinge, although it is not its appearance that invokes interest. It may be alloyed with a large amount of other elements to provide a variety of different properties such as chemical resistance, hardness and ductility. It occurs in its natural state as different oxides, depending on the valance state, with an average concentration of 5% in the earth's crust (6). The common occurrence and width of applicability has made iron, or rather steel, a popular material.

2.1. Steel production

Production of metallic iron on an industrial scale is mainly done by charging pelletized/sintered iron oxide enriched minerals together with carbon (coke) in a blast furnace (6) (8). In the blast furnace a stepwise reduction process of the iron oxide takes place at elevated temperatures by redox-reactions with mainly carbon, acting as reduction agent, and iron oxide as oxidant, the electron acceptor. This transfer of electrons transpires in many steps from which two principally important can be seen in **equations 2.1** and **2.2**. The oxidation of carbon is exothermic and provides the furnace with energy for heating and melting of the metallic iron and removes undesired moisture (6) (8).

$$3Fe_2O_3(s) + CO(g) \leftrightarrow 2Fe_3O_4(s) + CO_2(g) \qquad eq.2.1$$
$$\Delta H^0_{843\,K} = -30.05\ [kJ]$$

$$F\,e_3O_4(s) + 4\,CO(g) \leftrightarrow 3Fe(s) + 4CO_2(g) \qquad eq.2.2$$
$$\Delta H^0_{843\,K} = -44.478\ [kJ]$$

The molten iron, called pig iron, is now rich in carbon as well as sulphur, coming from the coke. Therefore, it must be further refined to make it useful as a material. Sulphur refining largely takes place in the torpedo car or ladle since the low oxygen potential environment favours its removal. The torpedo car is a transportation vessel for the molten pig iron from blast furnace to the basic oxygen furnace in which further refining is done. The basic oxygen furnace is so called because of the basic slags/refractory and high oxygen potential environment. By blowing large amounts of oxygen, dissolved carbon is oxidized in an exothermic reaction as carbon dioxide is produced, **equations 2.3** and **2.4**.

$$[C]_{Fe} \leftrightarrow C(gr) \qquad eq.2.3$$

$$\Delta G^0 = 22.594 - 42.258\,T \left[\frac{J}{mol}\right]$$

$$C(gr) + O_2(g) \leftrightarrow CO_2 \qquad eq.2.4$$

$$\Delta G^0 = 394762 - 0.836\,T \left[\frac{J}{mol}\right]$$

Moreover, the basic oxygen furnace provides an opportunity for phosphorus removal after which the pig iron is called crude steel. Further processing will then be conducted in the ladle. Depending on what quality of steel that is to be produced measures such as alloying, vacuum degassing and deoxidation can be taken. The steel is then solidified either continuously or in batches (8) (6).

A major part of all iron is produced in this fashion making the blast furnace the dominant process route. This is mainly due to the economic advantage over other process routes. On the other hand, it carries a hidden cost as it commits two tons of carbon dioxide to the atmosphere for each ton of steel produced. This is an emission quantity seen in modern integrated steel plants, in Sweden, while the global average rests even higher (5). Recycling of steel has therefore become popular as it is both economical and environmentally friendly. Reports, however, indicate that the global demand for steel cannot and will not be satisfied with only steel scrap in any near future (5). A forecast, made by SSAB, of steel demand and the raw material used can be seen in **figure 2.1**. Recycling will satisfy a relative larger portion of demand in the 2050, however, virgin material must be continuously added to feed the growing total demand. It will therefore be relevant to explore alternative reduction routes.

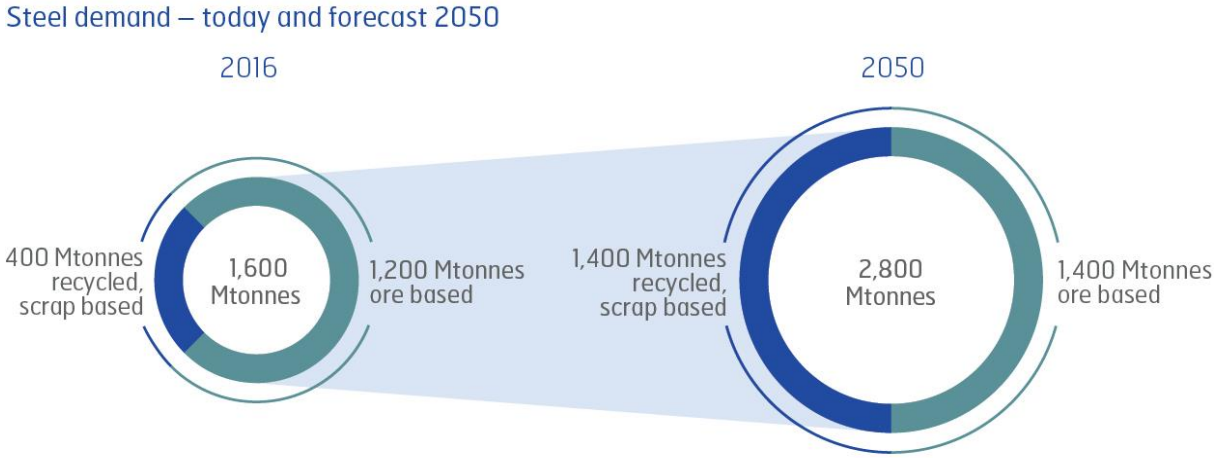

Figure 2.1 Projection of raw material source distribution for ironmaking in 2050 (8)

2.2. Direct reduction of iron oxides

In contrast to the blast furnace some reactors operate at lower temperatures to produce a solid state iron product in one step. A reduction gas is introduced into a shaft type furnace were it interacts with the iron oxide through a redox reaction. The product is called direct reduced iron or DRI for short, other terminology like bloom iron or sponge iron, from its porous sponge-like morphology, is also common (8) (6).

Solid state reduction enables an energy efficient production but offers little in the way of impurity removal, as the otherwise kinetically efficient liquid-liquid interface reactions are non-existent. Therefore, high quality raw material, usually pellets, with low concentrations of gangue is usually preferable from an economic and technical standpoint. Creating a high quality pellet, however, demands that the pellet producer spends more energy on mineral processing which directly translates to higher costs for the steel producer as these DR-grade pellets are sold at a premium (9).

The pellet was initially engineered to increase the efficiency of the blast furnace. However, pellets optimized for direct reduction have also been developed, the DR-grade pellet. Different grades of pellets are produced by adding different coating components such as limestone, dolomite and silica. High melting point additions decrease sticking problems that may arise in the DR-process. Furthermore, additions can be optimized to match slag requirements such as basicity in succeeding process steps. A desired slag composition might even be achieved without or with little slag additions. Such pellets are called self-fluxing (8) (6).

2.3. The reduction gas

Natural gas has been used successfully in direct reduction furnaces, e.g. the Midrex system. Such processes have enjoyed an economic advantage to the blast furnace route in countries were natural gas is readily available at a cheap price. Natural gas, consisting of hydrocarbons, can, however not be used directly and requires reformation before usage. Reformation is the process of cracking natural gas into more fundamental molecules, hydrogen H_2 and carbon monoxide, CO. Hydrogen reduction, seen in **equations 2.5** and **2.6** can be described in a similar fashion as carbon monoxide reduction, presented above in **equation 2.1** and **2.2**.

$$3Fe_2O_3(s) + H_2(g) \leftrightarrow 2Fe_3O_4(s) + H_2O(g) \qquad eq.2.5$$
$$\Delta H^0_{843\,K} = 6.440\ [kJ]\ (6)$$

$$Fe_3O_4(s) + 4\,H_2(g) \leftrightarrow 3Fe(s) + 4H_2O(g) \qquad eq.2.6$$
$$\Delta H^0_{843\,K} = 101.482\ [kJ]\ (6)$$

The large difference in enthalpy between carbon monoxide and hydrogen reduction is substantial. Hydrogen reduction is endothermic whilst carbon monoxide reduction is not. This energy sink can be partially offset, at low temperatures around 773 **[K]**, by the water-gas shift reaction, seen in **equation 2.7**

$$CO(g) + H_2O(g) \leftrightarrow CO_2(g) + H_2(g) \qquad eq.2.7$$
$$\Delta H^0_{298\,K} = -41.4\ kJ\ (6)$$

However, for steel makers aiming to produce a fossil free product this is a fundamental difference that should be addressed.

2.4. The HYBRIT-initiative

In 2015 the Swedish government declared that Sweden is to be a fossil free nation by 2050, a vision that pressures its industries into adopting fossil free solutions (10). This is particularly an issue for the steel industry and especially SSAB, which with its two blast furnaces is one of the single largest net producers of carbon dioxide in Sweden (5). To join in this vision a joint venture between the companies SSAB, Luossavaara-Kiirunavaara AB (LKAB), a pellet producer and mining company, and Vattenfall, an energy company, was announced in 2016 with the primary goal of eliminating carbon as the main reducing agent in steelmaking and thus making the blast furnace route obsolete (5). This is to be done by using hydrogen gas and as such the joint venture was called Hydrogen Breakthrough Ironmaking Technology (HYBRIT). When hydrogen is produced by the process of electrolysis with power from renewable sources and then used as reducing agent the theoretical carbon footprint of steel production is nil.

Vattenfall will provide necessary technological advancements in the field of electrolysis and deliver the energy to crack water. LKAB will develop a fossil free hydrogen DR-grade pellet which together with the Vattenfall-produced hydrogen will be used by SSAB in a shaft type furnace to produce low carbon DRI which is to be melted in a succeeding electric arc furnace (EAF) process.

2.5. The electric arc furnace

At the basic level the EAF can be described as an advanced melting machine. As seen in the schematic EAF drawing presented in **figure 2.2** the EAF is a container consisting of an outer water cooled steel shroud (blue), an inner protective refractory lining (green) typically magnetite, graphite electrodes (white) and a power source. In **figure 2.3** a newly tapped electric arc furnace, with the electrodes in a raised position, can been seen.

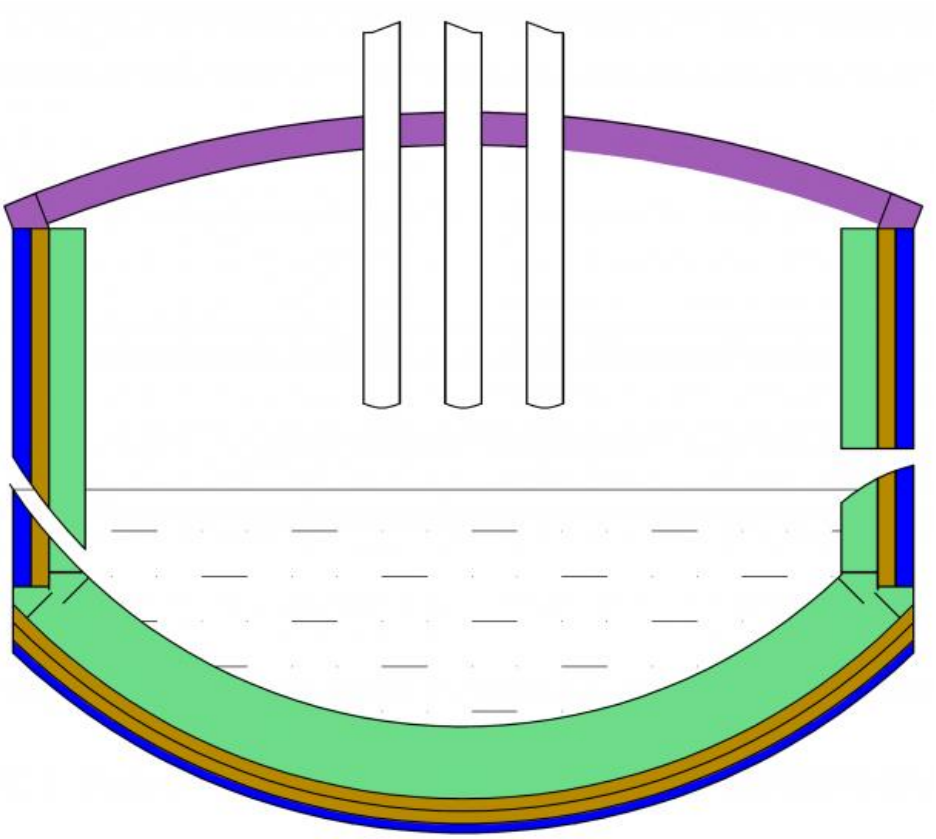

Figure 2.2 Schematic drawing of an EAF (11)

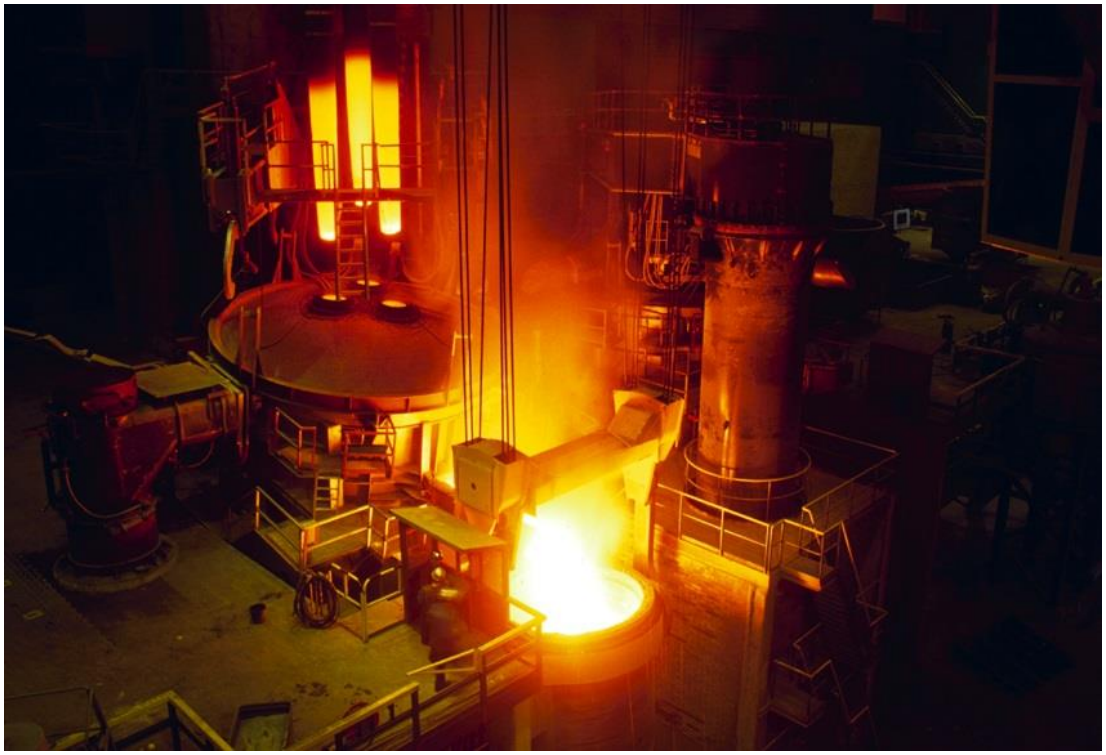

Figure 2.3 Operational EAF with three glowing electrodes in the upper left corner (12)

Buckets are used to load the furnace with raw material, usually scrap and/or pig iron or DRI (8) (6). There are two types of electric arc furnaces, one using direct current (DC) and one using alternating current (AC) and the AC type is predominantly used today. In a simple AC power system, current as well as electric potential, i.e. the voltage, follows the same sinusoidal wave pattern. Heat is generated as power is fed to the electrode and the sinus wave reaches a critical electric potential for electric discharge. The electric discharge heats up adjacent gas, forming a plasma which then conducts electricity into the raw material. This is the basic principle of creating an electric arc. However, current requires a closed loop in order to flow. Three phase power allows for a transient electric potential between three electrodes where each electrode represents one specific phase. Current flows between the electrodes as electric arcs are ignited on the raw material, serving as a conductor until another arc is lit on a different electrode. The main portion of heat is delivered by thermal radiation (8).

The theoretical energy requirement for melting of iron is 389 **[kWh/ton]** (13). A common EAF, however, spends around 650 **[kWh/ton]** (14). The difference consists largely in losses related to: the power source, the off gas (45-50%), as well as heat conduction and radiation (50%) (14). Work has been done to decrease the difference between the theoretical and practical energy consumption and as such it has steadily declined.

It has been found that the loss due to heat radiation can be lowered by increasing the efficiency of the electric arcs. The efficiency of electric arc heating varies depending on the environment in the furnace, most notably the presence of a foaming slag.

2.6. Electric arc furnace slag

Slags are an important aspect to many metallurgical processes. Sometimes its importance is neglected and this can prove to be a costly mistake e.g. according to A.N. Makarov the efficiency of the electric arc can be increased from 47% to 76% depending on the presence of a foaming slag and the height of the foaming slag (15).

Foaming slags accomplish to save energy by covering the electrodes, submerging the electric arcs into the foam. This reduces radiation of the arcs onto the refractory walls which in turn decreases the amount of heat that needs to be transported away by the water cooled steel shroud. Furthermore, a foaming slag protects the electrodes, reducing the rate of deterioration, something that has become more important as the global graphite electrode price surge continues to unfold (16).

A steelmaker that is interested in a foaming slag praxis will find himself involved with variables such as viscosity, surface tension, furnace geometry, gas generation/introduction in the steel bath (8). How

the interplay between these variables is and the mechanisms involved is currently not fully understood. However, it is accepted that viscosity and surface tension of a slag is dependent on slag composition (8). Some industrial EAF-slags can be seen in **table 2.1**.

Table 2.1: Some industrial EAF-slags in weight percent

Ref.	CaO	SiO_2	Al_2O_3	MgO	FeO	Fe_2O_3	P_2O_5	MnO	Free CaO
(17)	29.5	16.1	7.6	5	-	32.56	0.6	4.5	-
(18)	24.4	15.4	12.2	2.9	34.4	-	1.2	5.6	-
(19)	23.9	15.3	7.4	5.1	42.5	-	-	4.5	0.5

Even though there is some variation to the compositions they are designed with aspect to some particular parameters. Firstly, steelmakers strive toward having a slag with MgO-saturation as the refractory usually is made of magnesite or dolomite. Thermodynamically it is preferable to have MgO-saturation as otherwise the slag would corrode the refractory lining leading to higher maintenance. Having a basic slag, i.e. larger fraction of basic components such as CaO compared to acidic, e.g. SiO_2, also helps. Secondly, as mentioned above, the slag should possess properties that provide good underlying conditions for foaming. In **figure 2.4** a schematic pseudo-ternary phase diagram is presented (8).

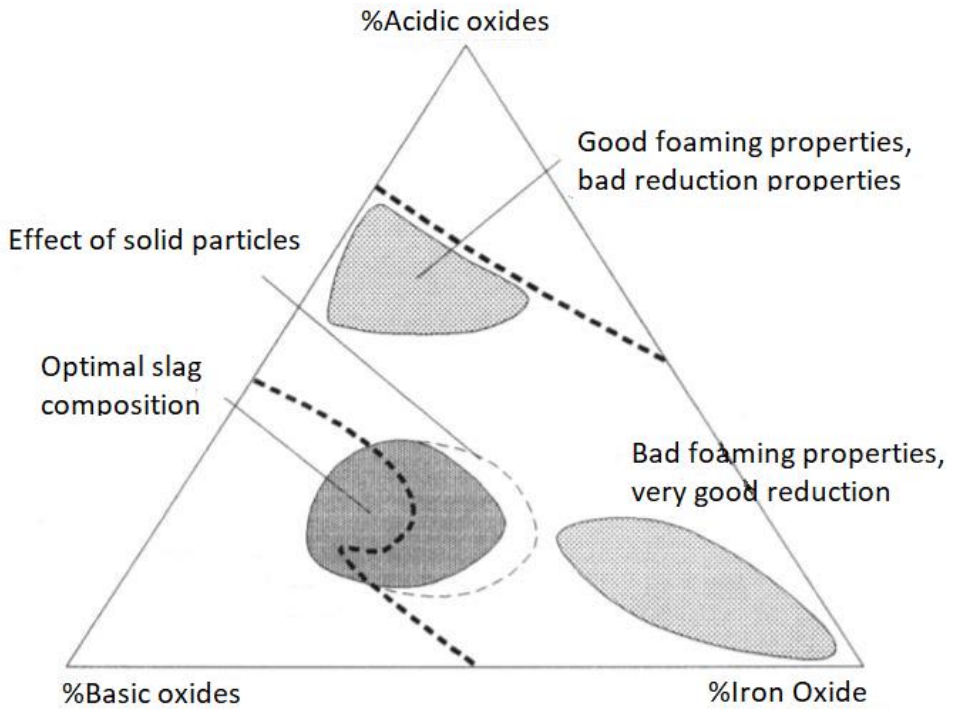

Figure 2.4 Schematic diagram displaying how foaming properties is dependent on slag composition (8)

Instead of displaying phases, however, a relationship between composition and foaming conditions is described. Thirdly, the slag should provide suitable conditions for the removal of harmful trace elements, such as phosphorus. The importance of this ability is dependent on the raw material that is charged. When pure scrap is melted this is rarely an issue, however, as the EAF is combined with DRI the electric arc furnace ceases being just an advanced melting machine. Instead it should also be looked upon as another opportunity for steel refinement.

2.7. Phosphorus removal

Phosphorus is an unwanted trace element present in the iron ore. It is found at varying concentration depending on the geographical location from where the iron ore was extracted. Concentrations at lower levels than in the ore should be reached to create a commercially viable steel and thus its removal should be emphasized in any steelmaking process. Phosphorus is associated with strong detrimental effects on ductility causing embrittlement. Although, it should be remembered that phosphorus provides benefits in machinability and strength. This is not the only balance that should be investigated. The amount of removed phosphorus is proportional to the amount of slag needed to remove it. Low phosphorus concentrations, therefore, might prove economically inefficient as cost arises with increased amounts of slag additions and then with the additional energy required for heating of this larger mass.

Phosphorus removal occurs, in the traditional blast furnace route, during the converting of pig iron into crude steel. Thermodynamically this only partially makes sense. Phosphorus reacts with oxygen to form P_2O_5, displayed in **equation 2.8** (20).

$$P_2(g) + \frac{5}{2}O_2(g) \leftrightarrow P_2O_5(l) \qquad eq.2.8$$

$$\Delta G^0_{P2O5} = -1585736 + 579.48\left[\frac{J}{mol}\right]$$

The equilibrium constant, K, can then be written as the activity fraction

$$K = \frac{a_{P_2O_5}}{{a_P}^2 * {a_O}^5} \qquad eq.2.9$$

and as

$$K = \exp\left(\frac{-\Delta G^0_{P2O5}}{RT}\right) \qquad eq.2.10$$

These equations provide insight into the conditions that promote the removal of phosphorus namely: low temperature (**eq.2.10**), high oxygen potential (**eq.2.9**) and a low P_2O_5 activity. The activity of P_2O_5 in the slag has been of interest in the research of Somnath Basu. By using the dilute solution model the activity of P_2O_5 can be written according to Henry's law

$$a_{P_2O_5} = \gamma^0_{P_2O_5} * N_{P_2O_5} \qquad eq.2.11$$

where the mole fraction, $N_{P_2O_5}$, is defined as

$$N_i = \frac{n_i}{\sum_{j=i}^{N} n_j} \qquad eq.2.12$$

Where, n_i, is the molar amount of a substance. Somnath Basu investigated the effects of slag composition on the activity coefficient, $\gamma^0_{P_2O_5}$. The investigation resulted in a model predicting the activity coefficient as a function of a simple slag composition. Four oxides were considered: CaO, MgO, FeO and SiO_2. This model can be seen in **equation 2.13** where it is based on the ionic fractions of the respective species (21).

$$\log(\gamma_{P_2O_5}) = -8.172\boldsymbol{X_{Ca^{2+}}} - 7.169\,\boldsymbol{X_{Fe^{2+}}} - 1.323\,\boldsymbol{X_{Mg^{2+}}} + 1.858\,\boldsymbol{X_{SiO_4^{4-}}} + \frac{340}{T} - 11.66 \qquad eq.2.13$$

Basu's model indicate that CaO, MgO and FeO lowers the activity coefficient whilst SiO_2 increases it which is in line with established theory. However, Basu's alternative model based on molar fractions, **equation 2.14**, indicate that SiO_2 and CaO influence the activity coefficient in the same direction. This deviation from established theory was not further discussed.

$$\log(\gamma_{P_2O_5}) = -6.775\boldsymbol{N_{CaO}} - 4.995\boldsymbol{N_{FeO}} + 2.816\boldsymbol{N_{MgO}} - 1.377\boldsymbol{N_{SiO_2}} + \frac{1007}{T} - 13.992 \quad eq.2.14$$

Nevertheless, a slag suited for phosphorus removal is a slag rich in basic components especially CaO as it is most effective (21).

Thermodynamics is crucial for phosphorus removal. Every reaction process should carefully consider then underlying thermodynamics as without favourable conditions a reaction will not take place. However, even with sound thermodynamics a reaction can be stopped by kinetics. Phosphorus removal kinetics is dependent on stirring, temperature and most importantly slag-metal interactions. To allow for proper slag-metal interactions the slag should be liquid as kinetics in liquid phases is better than in solid phases. The melting temperature of a slag is decided by its composition. As slags are

described with for or more components, the resulting phase diagram will be more complex to the point where visual presentation is no longer possible. For a four-component slag a surface representation of the liquidus space can be made. In **figure 2.5** a pseudo-ternary $CaO - MgO - FeO - SiO_2$ phase diagram, at 1600°C, with belonging liquidus surface representation can be seen (22). Only the equilateral triangle, marked with the roman numeral 1 in the smaller rightmost diagram, should be considered and triangle to the left discarded. The lower axis represents the FeO content, in weight percent, in the slag, the right axis represents SiO_2 and the left axis a combination between CaO and MgO. Also, in the surface representation are MgO-saturation lines.

To summarize, a, for phosphorus removal, optimal slag should be liquid, i.e. located in the liquidus surface representation in **figure 2.5**, should provide a low phosphorus a activity coefficient, $\gamma^0_{P_2O_5}$, see **equations 2.9**, **2.11** and **2.13**, be MgO-saturation and should be within the optimal composition range balancing foaming and reduction properties **figure 2.4.**

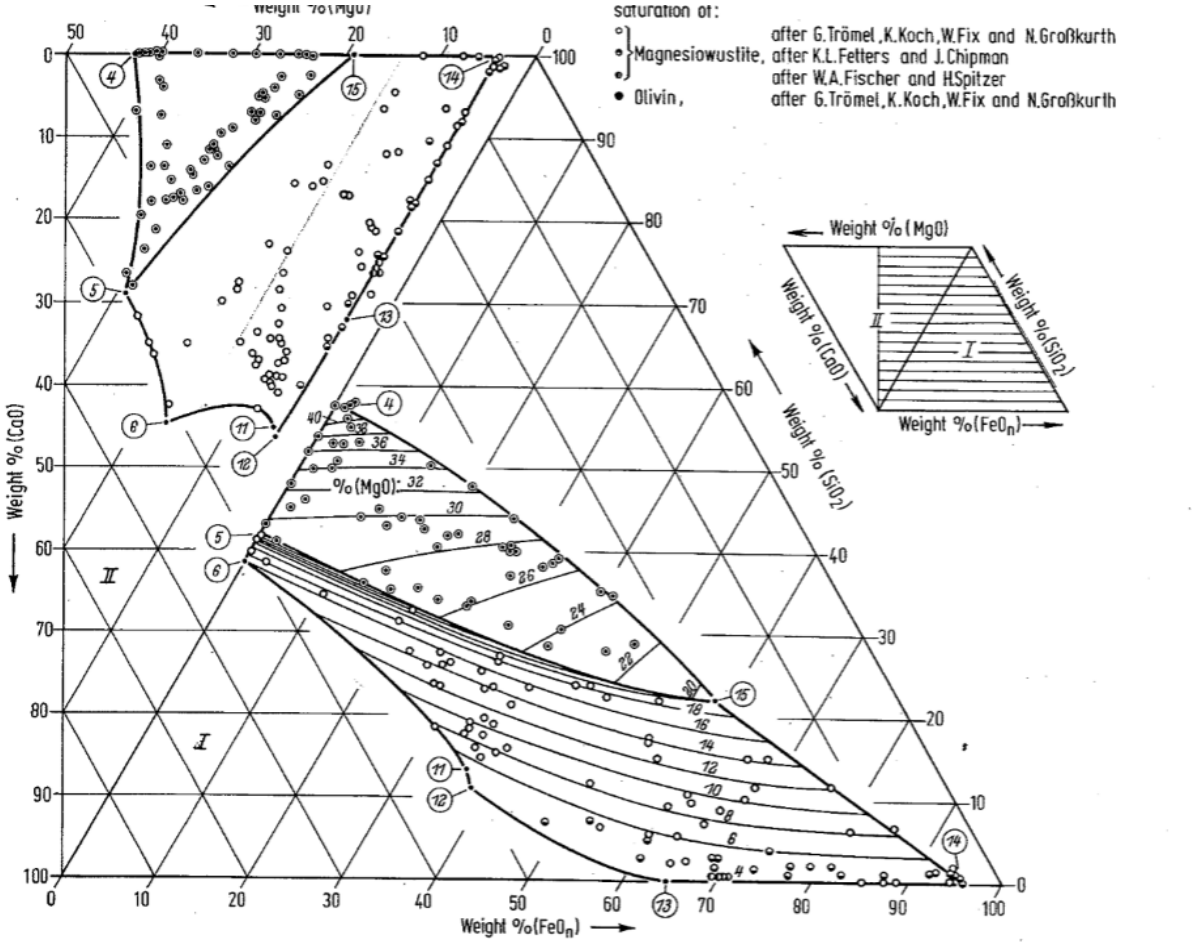

Figure 2.5 Pseudo-ternary phase diagram displaying the liquidus surface (22)

2.8. The cost of a slag

In order to construct a slag, to reach a target composition, slag formers need to be added. Just like any other material these slag formers comes with a cost. Some commonly used slag formers are burnt lime and dolomite. Burnt lime is a source of CaO which is imperative for phosphorus removal, as can been seen in Somnaths Basus model (21) while dolomite is a source of MgO. These slag formers are not pure, burnt lime having a composition of 95 **[wt%]** CaO, 2 **[wt%]** MgO, 1 **[wt%]** FeO and 2 **[wt%]** SiO_2 and dolomite: 58 **[wt%]** CaO, 40 **[wt%]** MgO, 1 **[wt%]** FeO and 1 **[wt%]** SiO_2 with costs of 1200 **[kr/ton]** and 2000 **[kr/ton]** respectively (23).

The slag must then be heated. The energy requirement for heating of the slag is decided by properties such as specific heat capacity, C_p, and heat of fusion for melting of the slag. Thus, the total cost of a slag can be described as having two parts the construction cost and the heating cost.

2.9. The dictionary attack method

Early in computer development a basic strategy for breaking encryption keys was developed. Rather simple by nature it was based on painstakingly testing every single possible combination to find the right one. As encryption keys become longer so does the time involved with breaking one, simply because of the amount of combinations increases non-linearly with every new variable added. This method, of testing every possible combination, is called the brute force method as it relies purely on the computational power of a device or cluster. Modern encryption keys are based on an amount of variables which is not practical, from a time perspective, to break by brute force. Even simple everyday passwords can be hard to break. It therefore did not take long before an improvement was made. Instead of trying every combination only the most probable combinations are tested. An everyday example might be to try “qwerty” to break a password. This is a high probability combination as those keys sits next to each other on the keyboard. Another example would be to gain information about the target. Knowing that the target has a dog called “Skip” might be helpful in breaching a person’s security. This more efficient method is called the dictionary attack method. Here, a dictionary is created containing information and high probability syllables and phrases. This dictionary enables the computer to make “smart” guesses at a computational lesser cost (24).

3. Method

Matlab (25) was used as an umbrella program to harbour the final 17 modules that carry out the computations. All calculations are based on the assumption of thermodynamic equilibrium.

3.1. Oxygen content calculations

To calculate the solubility of oxygen in a pure iron melt, in equilibrium with a slag phase, the FeO-activity was assumed to be the controlling factor and thus the reaction $Fe(l) + [O]_{1wt\%\,Fe} \rightarrow FeO(l)$ will be controlling.

The activity of FeO and the temperature were varied across a spectrum of 0.1-1 and 1773 -1923 **[K]** respectively, however, in subsequent modules only the data related to 1923 **[K]** was used, as this is a common tapping temperature for electric arc furnaces. The equilibrium constant was calculated using the case specific version of **equation 2.10** where the standard Gibb's function of formation for the reaction above was calculated from an aggregate of half reactions, **equations 3.1 to 3.4**.

$$Fe(s) + \frac{1}{2}O_2(g) \leftrightarrow FeO(s) \qquad eq.3.1$$
$$\Delta G^0 = -261182 + 62.93\,T\left[\frac{J}{mol}\right] (26)$$

$$Fe(s) \leftrightarrow Fe(l) \qquad eq.3.2$$
$$\Delta G^0 = 13807 + 7.633\,T\left[\frac{J}{mol}\right] (27)$$

$$FeO(s) \leftrightarrow FeO(l) \qquad eq.3.3$$
$$\Delta G^0 = 21748 - 3.277\,T\left[\frac{J}{mol}\right] (28)$$

$$\frac{1}{2}O_2(g) \leftrightarrow [O]_{1wt\%\,in\,Fe} \qquad eq.3.4$$
$$\Delta G^0 = -115750 - 4.63\,T\left[\frac{J}{mol}\right] (29)$$

The case specific equilibrium constant was set as the right hand side (RHS), **equation 2.11**, and the activity fraction as the left hand side (LHS), **equation 3.5**, where a_{FeO} is the activity of FeO, a_o the activity of dissolved oxygen and a_{Fe} the activity of iron in the melt.

$$K = \frac{a_{FeO}}{a_O * a_{Fe}}\ eq.3.5$$

The interaction between species was treated as non-ideal and thus data on the interaction parameters was gathered (30) (31). Furthermore, the activity of iron was assumed to be equal to unity. A comparison with "Thermo-Calc" calculations (32) proved this to be a sufficiently accurate assumption and **equation 3.5** could thereafter be rewritten as:

$$K = \frac{a_{FeO}}{a_O} \; eq. 3.6$$

In order to extract information regarding the weight percent of dissolved oxygen the denominator in **equation 3.6** was rewritten using the dilute solution model in conjunction with the Wagner-equation, **equation 3.7**.

$$logf_i = \sum_{j=i}^{N} e_i^j wt\% \, j \quad eq. 3.7$$

Resulting in the following expression, **equation 3.8**, where e_o^o is the oxygen-oxygen interaction parameter and $wtO\%$ the weight percent of dissolved oxygen in the steel melt.

$$K = \frac{a_{FeO}}{10^{-e_o^o * wtO\%} * wtO\%} \; eq. 3.8$$

Equation 3.8 posed an iterative problem as the variable $wtO\%$ could not be analytically extracted. A starting value of 0.00001 was attributed to the variable $wtO\%$ and was increased with 0.00001 in each iteration until the difference between the RHS and LHS was less than 0.1. The iso-activity lines were thereafter plotted with $wtO\%$ as a function of temperature.

3.2. Slag composition creation

To avoid pre-existing biases regarding the design of a slag system permutations of all possible slag compositions were created, with a step size of 1 **[wt%]**. Although, in order to decrease computation time requirements in later stages certain restrictions had to be put place. Some of these are to be treated only as safeguards from illogical or unwanted compositions e.g. a slag containing 100 **[wt%]** SiO_2, or a slags containing non-valid total percentages. Other restrictions chosen were: **[wt%]** MgO < 30, **[wt%]** FeO < 35, **[wt%]** SiO_2 < 40, 70 < **[wt%]** CaO < 10 and 1.1 < basicity. This practice reduces the number of compositions from orders of 10^6 to 10^4 so that a total of 26863 compositions were created.

The activity coefficient of P_2O_5 is then calculated for each composition, using Somnath Basu's model (21). To calculate the activity of P_2O_5 in the slag **equation 2.11** was used. This requires an assumption

regarding the equilibrium concentration of $\mathrm{P_2O_5}$ in the slag. The concentration was assumed to be 0.5 **[wt%]**. Furthermore, to make use of **equation 2.11** the mole fraction of $\mathrm{P_2O_5}$ is defined as:

$$X_{\mathrm{P_2O_5}} = \frac{wt\%\mathrm{P_2O_5} * M_{slag}}{100 * M_{\mathrm{P_2O_5}}} \quad eq.3.9$$

where M_{slag} is the weighted average molar weight of the slag and $M_{\mathrm{P_2O_5}}$ the molar weight of $\mathrm{P_2O_5}$.

3.3. Phosphorus content calculations

Calculations regarding the phosphorus content in a steel melt were carried out using equilibrium calculations similar to those in the oxygen content calculations. One difference being that the temperature was fixed. One temperature was tested, 1923 **[K]**, so that, instead of being a function of temperature phosphorus content was treated as a function of dissolved oxygen, which was determined by the activity of FeO, and of the activity of P_2O_5 in the slag phase. The activities were varied between 0.1-1 and in the magnitude of 10^{-23} -10^{-19} respectively. The computational domain was provided by extracting the minimum and maximum P_2O_5 activity in the preceding step.

By expanding the numerator of **equation 2.9** in accordance with the dilute solution model and the denominator according to the Wagner equation, the equation subject to calculations can be seen in **equation 3.10**.

$$K = \frac{\gamma^0_{P_2O_5} * X_{P_2O_5}}{(10^{e_P^O * wt\%O} * wt\%P)^2 * (10^{e_O^O * wt\%O + e_O^P wt\%P} * wt\%O)^5} \quad eq.3.10$$

Where $wt\%P$ is the dissolved phosphorus amount in the steel melt, e_p^o the phosphorus-oxygen interaction parameter and e_o^p the oxygen-phosphorus interaction parameter.

Similarly to **equation 3.8**, $wt\%P$ cannot be analytically extracted and must be iterated upon. **Equation 2.10** was set as the RHS and **equation 3.10** as the LHS. The standard Gibb's function of formation, used in the RHS, was calculated using **equation 3.4** and the following partial reactions:

$$P_2(g) + \frac{5}{2}O_2(g) \leftrightarrow P_2O_5(s) \quad eq.3.11$$
$$\Delta G^0 = -1585736 + 579.48\,T \left[\frac{J}{mol}\right] (20)$$

$$\frac{1}{2}P_2(g) \leftrightarrow [P]_{1wt\%\,in\,Fe} \quad eq.3.12$$
$$\Delta G^0 = -122173 - 19.25\,T \left[\frac{J}{mol}\right] (20)$$

$$P_2O_5(s) \leftrightarrow P_2O_5(l) \quad eq.3.13$$
$$\Delta G^0 = 51254 - 73.22\,T \left[\frac{J}{mol}\right] (20)$$

$Wt\%P$ was attributed a starting value of 0.0001 and was increased with 0.0001 for each iteration. When the difference was less or equal to 10^{-18} the solution was considered to be found. The activity of P_2O_5 was varied with a step size of 10^{-23}. For each step in P_2O_5-activity the entire range of $wt\%O$ was inserted, evaluating the corresponding amount of dissolved P for every combination of a_{FeO} and $a_{P_2O_5}$. It should be noted that information regarding the interaction parameter e_P^P was not available and the P-P interaction was treated as ideal, i.e. $e_P^P = 0$.

As stated earlier, the activity of FeO provides the concentration of oxygen in the melt. This oxygen content in combination with an activity of P_2O_5 yields the equilibrium phosphorus content. This means that a slag can be considered an effective vessel for phosphorus removal only if it meets one of the required combinations.

3.4. Slag evaluation

The 26863 slags created were evaluated in "Thermo-Calc", using the SLAG4 database (33). Information regarding the fraction of liquid phase, activity of FeO, fraction of CaO solid phase, fraction of MgO solid phase and other complex solid phases, e.g. $2CaO * SiO_2$, was extracted. An API-interface called "TC-Toolbox" was utilized in this process. The slag weight was calculated from a mass balance between two initial phosphorus concentrations, 250 ppm and 125 ppm, in two theoretical raw materials and a slag where the P_2O_5 assumption made above was applied. An initial screening was done, although as different processes demand different properties from the slag system different requirements can be imposed onto the system. The requirements chosen were MgO-saturation, a melted slag and a low phosphorus equilibrium. MgO-saturation was ensured by imposing the restriction that the amount of solid fraction MgO must be above zero. The amount of solid fraction was then strongly limited by the requirement of a liquid slag, defined as a liquid fraction above 0.995 and by limiting solid phases, other than MgO, to 0%. The low phosphorus equilibrium was defined as when the equilibrium amount of phosphorus in the steel melt was below or equal to 0.09 **[wt%].**

Furthermore, the integrated molar specific heat capacity of the slag compositions was evaluated using "TC-toolbox" and discrete integration or if many slags were to be evaluated a standard value of 12000 **[J/mol]** was attributed for heating from 298 **[K]** to 1923 **[K]** as C_p-evaluation was computationally expensive. Heat of fusion for all the slags was set to 17939 **[J/mol]** a value extracted from "Thermo-Calc" for one composition (33).

This served as the fundamental data for calculations on the heating costs of the slags. The cost of electricity was set to 0,4 **[SEK/kWh]** and the efficiency of the arc to 0.47. Moreover, the total slag cost is an agglomerate of construction cost, i.e. the cost of adding slag formers, and heating cost. In order to analyse the cost associated with slag construction, two theoretical slag formers were used:

a pure FeO and a pure SiO_2 addition. The FeO addition was attributed a cost of 78.43 **[USD/ton]**, which is the cost of MBIOI-62 an index for DR-grade pellets (34), with a conversion rate of 8.2652 **[SEK/USD]** as of 2018-03-05 (35) and SiO_2 was attributed a weighted average depending on slag composition to omit its impact on construction cost.

Construction was calculated in three ways: the equilibrium, the "constructed" and the DRI-based way. Equilibrium construction is based on that all slag formers are pure while the constructed way does not. The DRI-based construction are slags made from an initial slag that has a weight 34.1587 **[kg/ton]** of steel and a composition of 33.7855 **[wt%]** CaO, 22.688 **[wt%]** MgO, 13.1936 **[wt%]** FeO and 30.3329 **[wt%]** SiO_2. The important difference being that the "constructed" slag can be treated as a two-slag praxis and the DRI-based a one-slag praxis. The different construction types are summarized in **table 3.1**. The initial P_2O_5-assumption was released for the "constructed" and DRI-based ways compared to the equilibrium. Optimization was then done based on slag weight.

Table 3.1 Summary of construction ways

Type of construction	Base assumption	Slag praxis
Equilibrium	All slag formers are pure	Theoretical
Constructed	Two real slag formers	Two-slag praxis
DRI-based	Initial slag (34 kg)	One-slag praxis

4. Results

The results will be presented in the order that the data was needed to cater for further calculations. First calculations regarding oxygen content will be presented as this is a precursor for the phosphorus calculation, as it inherently relies on oxygen activity data, see **equation 3.10**. Thereafter, the phosphorus results will be presented. These two together provide the basis for allowing connections to be made between slag composition and phosphorus concentration in the melt. How these slag compositions behave is presented afterwards in two batches of requirements.

4.1. Oxygen and Phosphorus calculations

In **figures 4.1** and **4.2** results regarding dissolved oxygen in a steel melt is presented. Oxygen content varies as a function of temperature in **figure 4.1.** With an increase in temperature follows a non-linear increase in oxygen content, higher temperatures provide higher oxygen potential. Also in **figure 4.1** multiple lines are to be seen. These are the iso-activity lines of FeO ranging from 0.1 in the bottom and 1 at the top, with step size of 0.1, larger activity facilitates a higher oxygen content. As this data is the foundation of all subsequent calculations the step size was needed to be decreased for more accurate calculations. Each blue data point represents one FeO activity in **figure 4.2**. Also, calculations, with the smaller step size, was only made at one temperature, 1923 **[K]**, to decrease the complexity and to provide the possibility of graphical representation in later stages, as otherwise four variables would have been in play simultaneously.

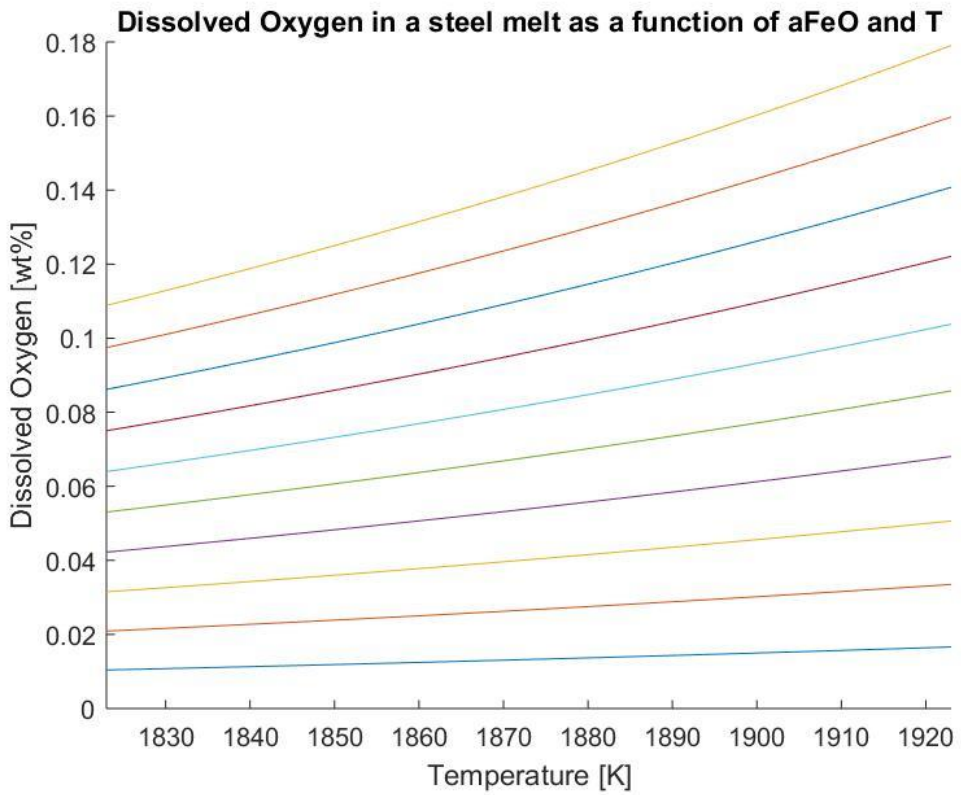

Figure 4.1 Oxygen content in [wt%] as a function of temperature [T] with Iso-activity lines of FeO from 0.1-1

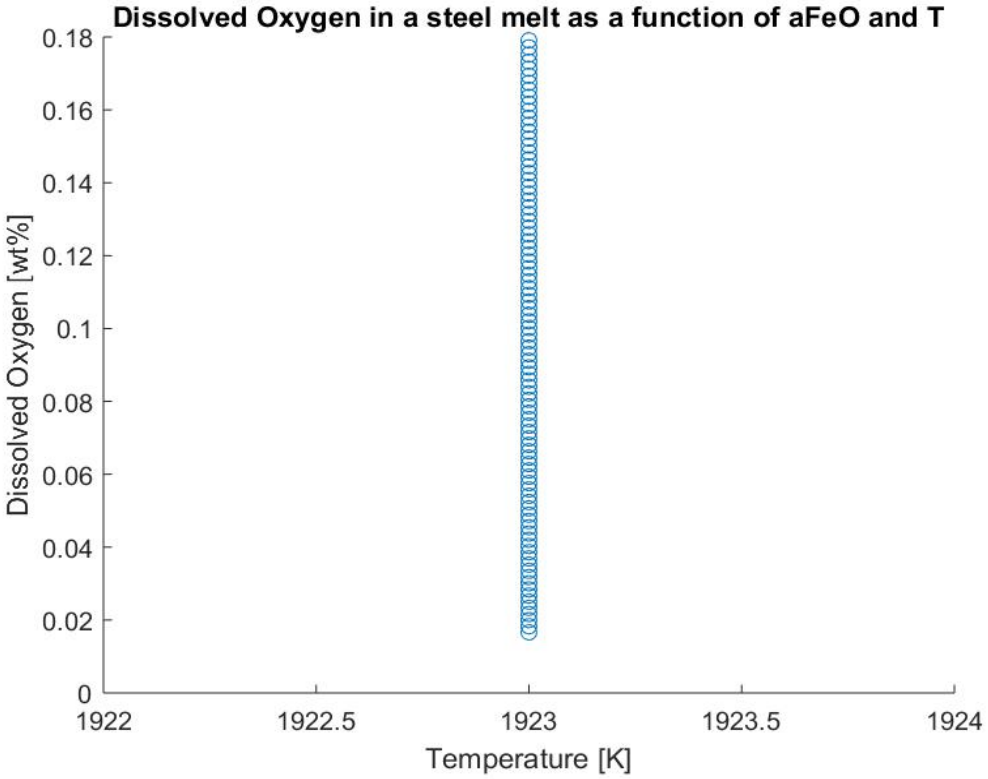

Figure 4.2 Oxygen content in [wt%] as a function of activity of FeO from 0.1 -1 at 1923 [K]

As stated above, phosphorus content in the steel melt is dependent on the oxygen potential, decided by the activity of FeO, but also on the activity of the reaction product P_2O_5, this can also be seen in **equation 3.10**. Therefore, in **figure 4.3**, phosphorus content in a steel melt is presented as a function of both the activity of FeO and P_2O_5. This results in a plane in the 3rd dimension with a fixed temperature of 1923 **[K]**. At low oxygen contents, i.e. low FeO-activity, the dissolved phosphorus content rises exponentially. By limiting the phosphorus-axis to 0.015 **[wt%]** the relation between phosphorus content and activity of P_2O_5 is made observable in **figure 4.4** and displays a parabolic proportionality.

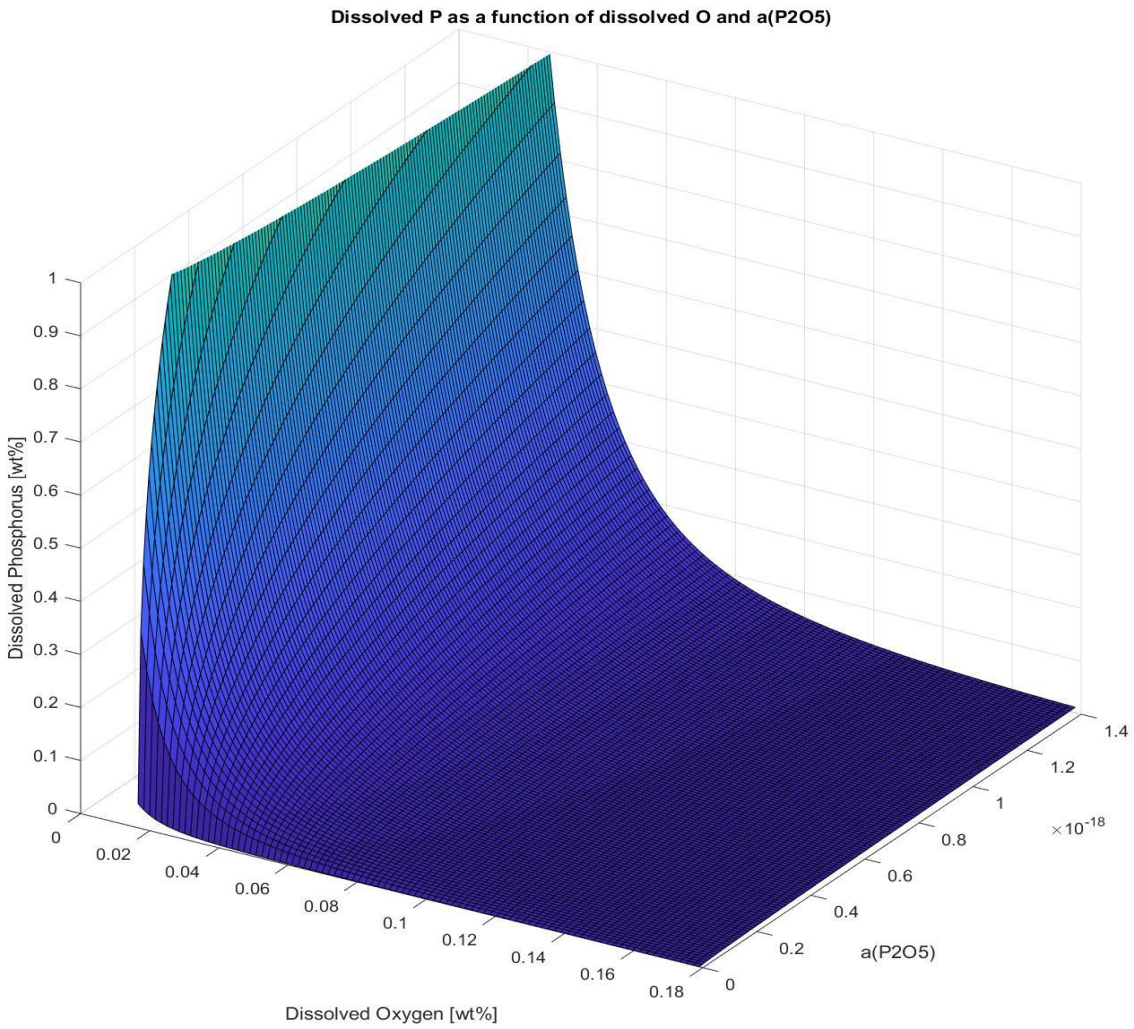

Figure 4.3 Dissolved phosphorus [wt%] as a function of dissolved oxygen [wt%] and activity of P_2O_5

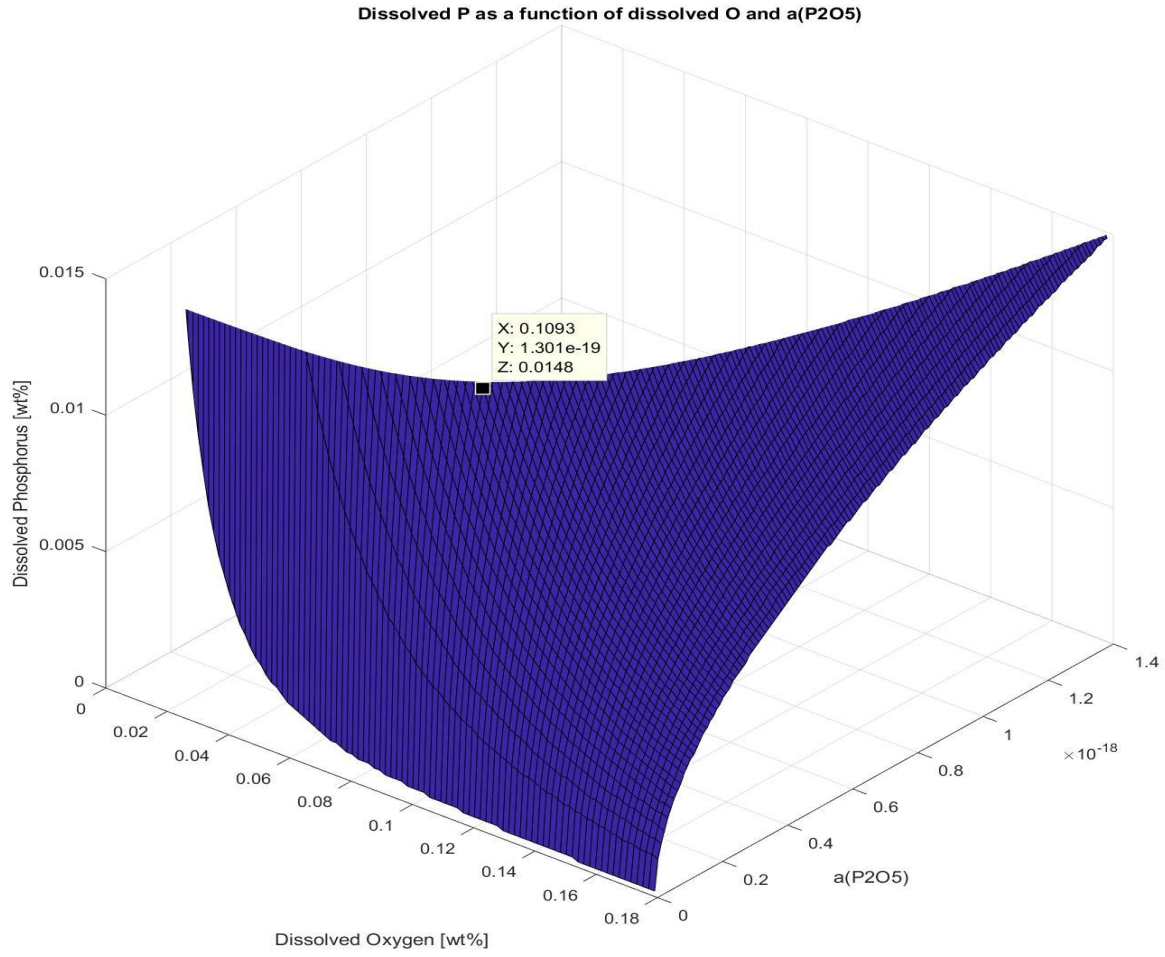

Figure 4.4 Dissolved phosphorus [wt%] as a function of dissolved oxygen [wt%] and activity of P_2O_5 with limited phosphorus axis at 0.015 [wt%]

By eliminating the phosphorus axis in **figure 4.4** the P_2O_5-activity and dissolved oxygen content relation can be studied, see **figure 4.5**. The curvature represents the iso-potential for phosphorus more specifically 150-145 ppm of dissolved phosphorus. This range comes from the step size chosen earlier which gives the fineness of the "mesh" or computed grid points. However, this curvature can be interpreted as the combination required to reach a certain phosphorus content. A grid point is made visible in the figure. This displays that a combination of 0.1203 **[wt%]** oxygen in the steel melt and a P_2O_5-activity of 2.001e-19 will provide, when in equilibrium, a phosphorus content of 146 ppm. This diagram, therefore, graphically displays how the condition of a low phosphorus equilibrium can be achieved.

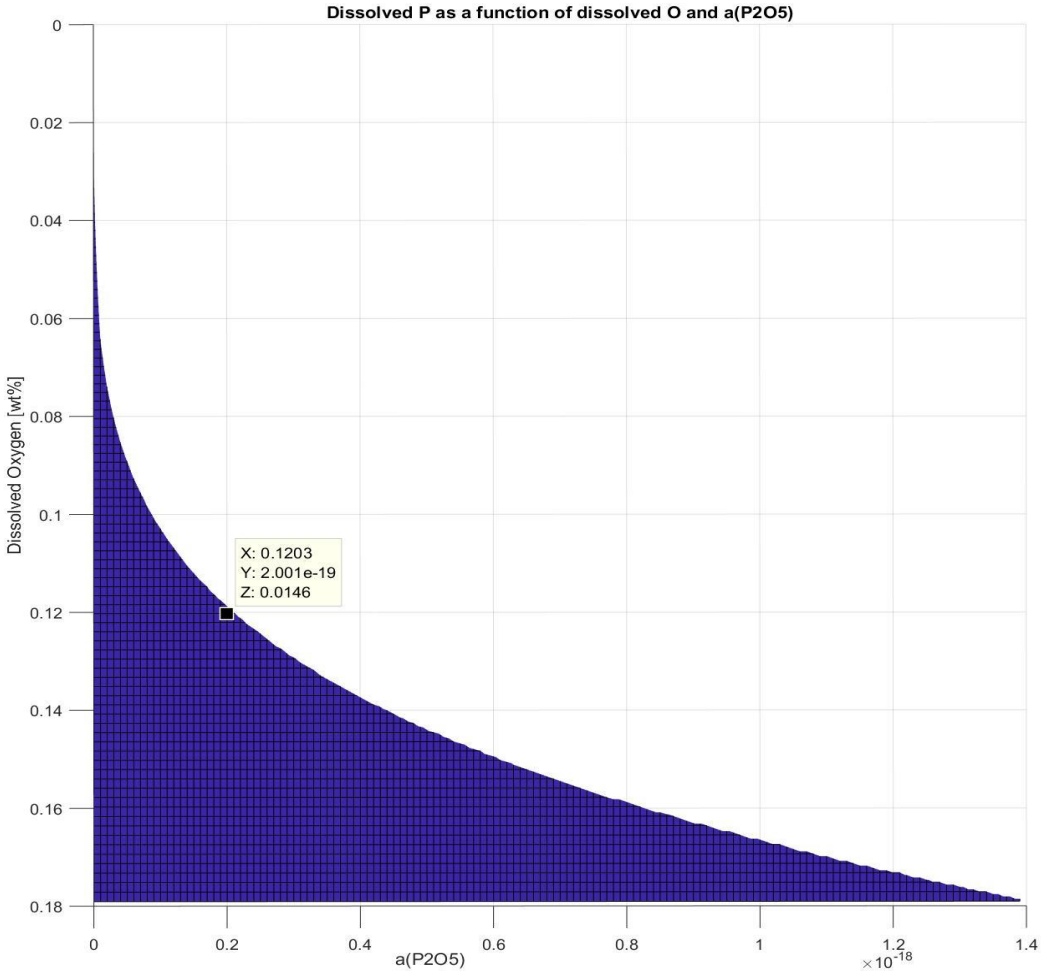

Figure 4.5 Dissolved oxygen [wt%] and activity of P_2O_5 at iso-phosphorus potential (146-150 ppm)

4.2. MgO-unsaturated slags

Two batches of criteria were tested. First the batch with the lesser amount of criteria will be presented. These requirements were: low phosphorus equilibrium, i.e. $wt\%P < 0.09$, and a liquid slag at 1923 **[K]**. The phosphorus equilibrium was decided from the grid points in **figure 4.5** and the slag weight from a mass balance.

Out of the 26863 slag compositions created 1564 passed these criteria. The compositions varied within a large composition range. It should be noted that "Thermo-Calc" failed to successfully evaluate 881 compositions and they were, thus, discarded without evaluation.

In **figure 4.6,** slag amount, defined as **[kg/ton]** of steel, as a function of dissolved phosphorus, based on an initial concentration of 250 ppm, can be seen, where each blue data point represents a slag composition. A larger slag amount follows from lower concentrations of dissolved phosphorus in a linear fashion.

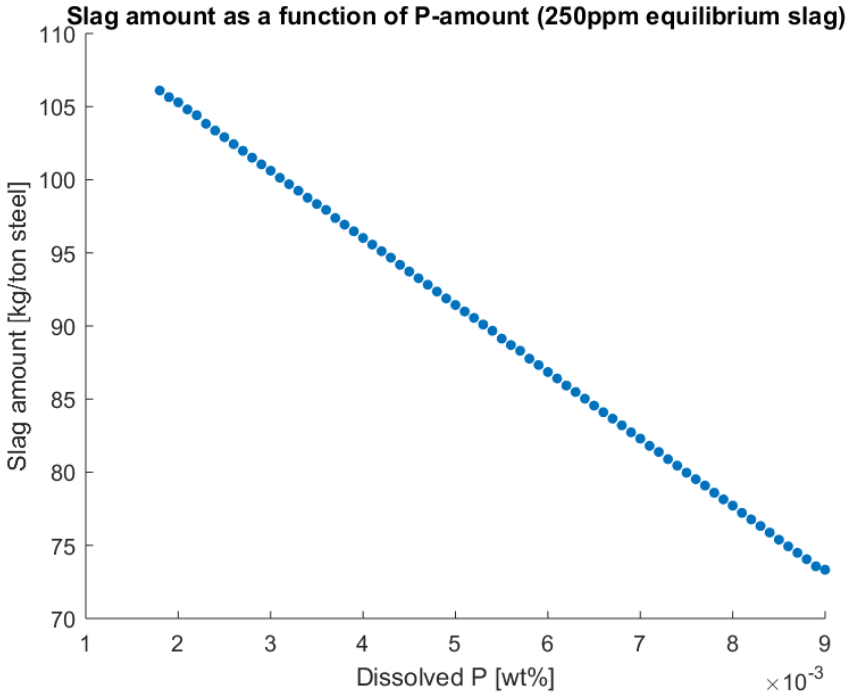

Figure 4.6 Slag amount [kg/ton] for slag different compositions as a function of dissolved phosphorus at an initial phosphorus concentration of 250 ppm (equilibrium construction)

The impact of initial phosphorus concentrations on required slag weight can be seen in **figure 4.7**. By doubling the initial phosphorus amount, red data points based on 125 ppm, the slag weight required for phosphorus removal is larger.

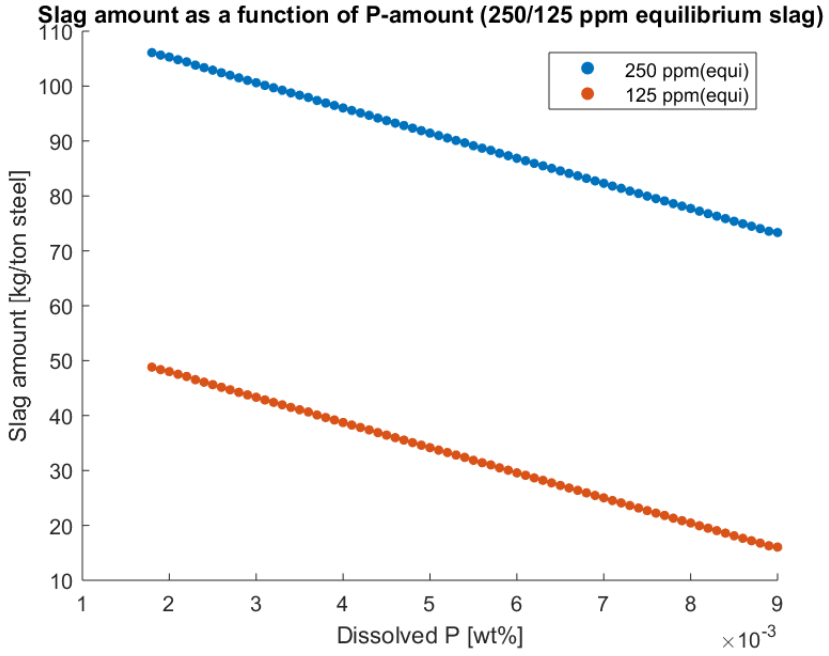

Figure 4.7 Slag amount [kg/ton] for different slag compositions as a function of dissolved phosphorus at two initial phosphorus concentrations 250 ppm and 125 ppm (equilibrium construction)

The figures above are based on the equilibrium construction of a slag, i.e. when all slag formers are pure. **Figure 4.8** displays the difference between the equilibrium and the constructed way, marked with red data points. For the constructed slags the linear relationship between dissolved phosphorus and slag weight is no longer to be seen, instead an exponential proportionality can be sensed. This is made more apparent in **figure 4.9** which is an optimized version of **4.8**, meaning that compositions that require a lower amount of slag for a certain phosphorus equilibrium outcompetes compositions that require a larger slag weight for the same phosphorus content. Optimization can also be described graphically as the lower limit of the red field in **figure 4.9**. Furthermore, constructed slags generally require more mass than equilibrium slags. This also holds true for the raw material with lower initial phosphorus concentration, see **figure 4.10** where a comparison can be seen.

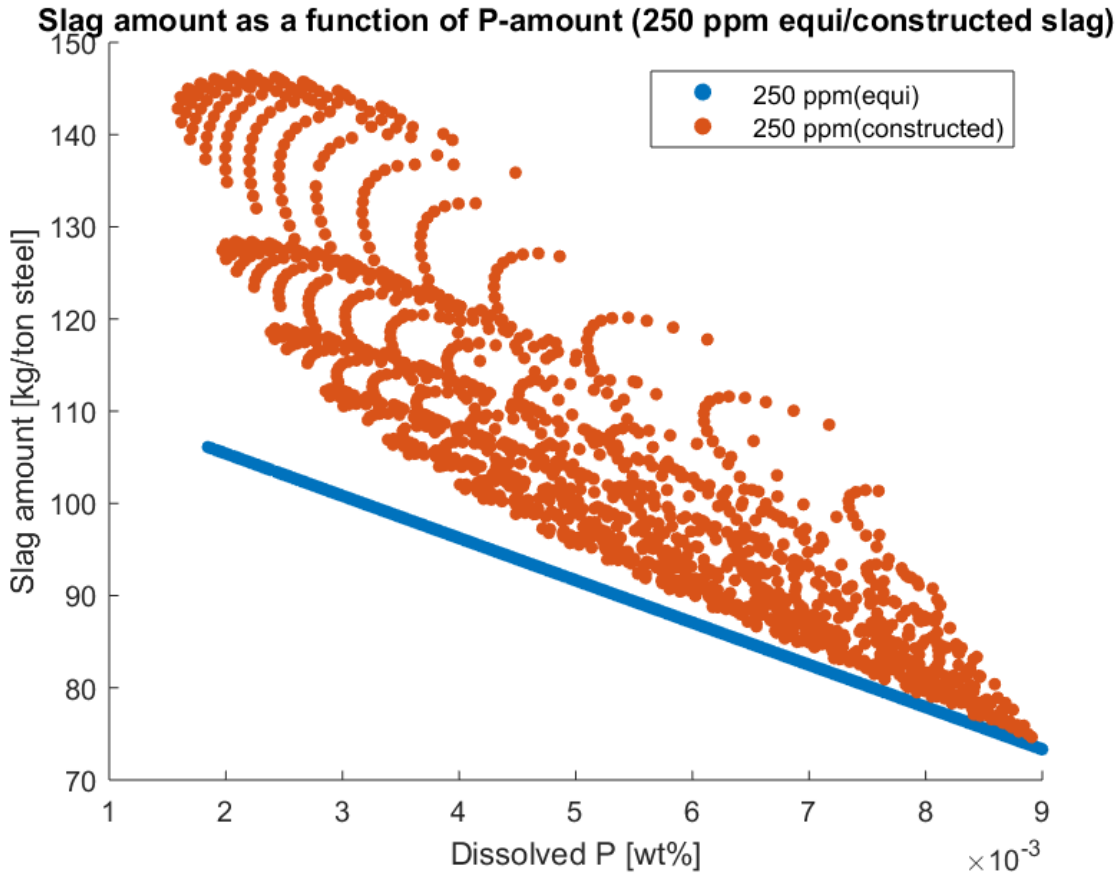

Figure 4.8 Slag amount [kg/ton] for different slag compositions as a function of dissolved phosphorus at an initial phosphorus concentration of 250 ppm (equilibrium and "constructed" slags)

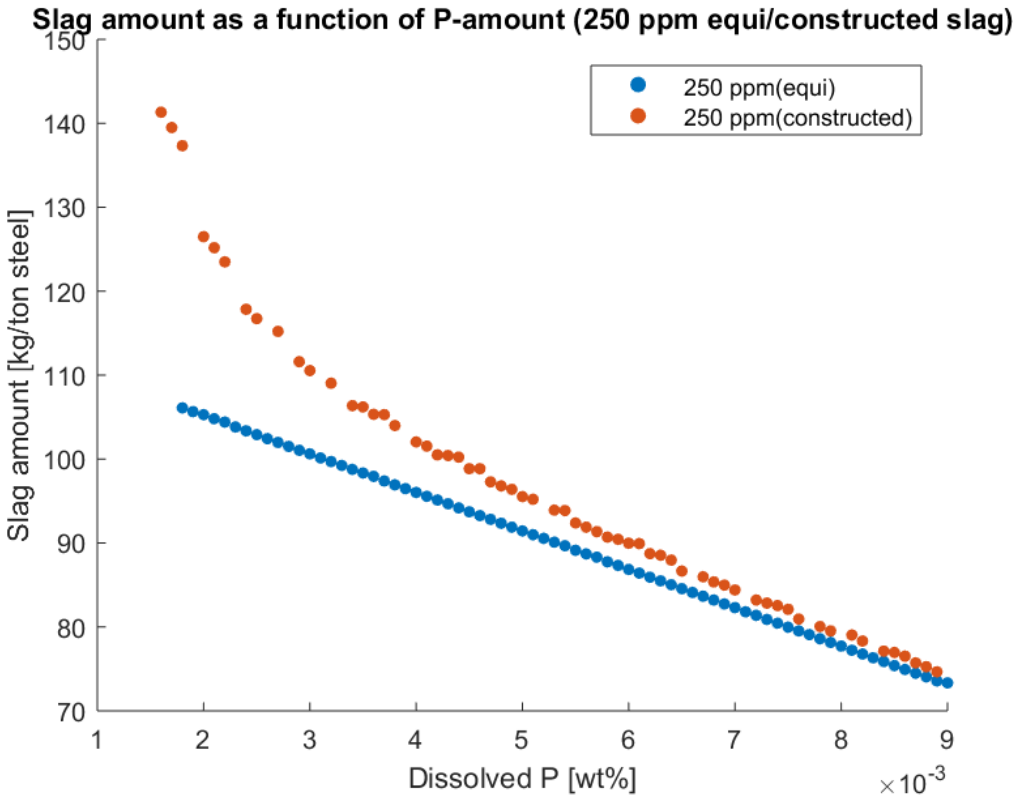

Figure 4.9 Weight optimized slag amount [kg/ton] for different slag compositions as a function of dissolved phosphorus at an initial phosphorus concentration of 250 ppm (equilibrium and "constructed" slags)

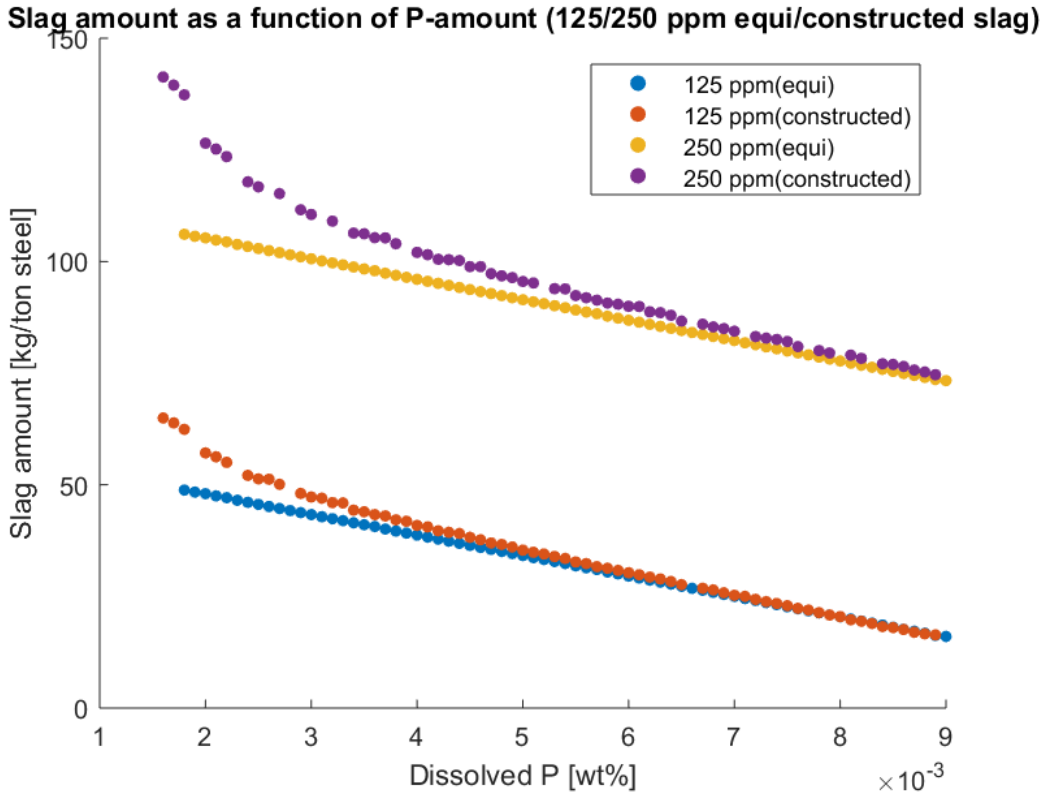

Figure 4.10 Weight optimized slag amount [kg/ton] for different slag compositions as a function of dissolved phosphorus at two initial phosphorus concentrations 250 ppm and 125 ppm (equilibrium and "constructed" slags)

By observing **figure 4.11**, where slag weight has been translated into slag cost, defined as **[kr/ton]** of steel, it is seen that slag cost, similarly to slag weight, is proportional to the amount of dissolved phosphorus. The slag amount and slag weight follows the same curvature. Having a raw material with less initial phosphorus leads to reduced slag cost, which can be seen when comparing the red data points, 125 ppm of initial concentration, and the blue data points, 250 ppm of initial concentration.

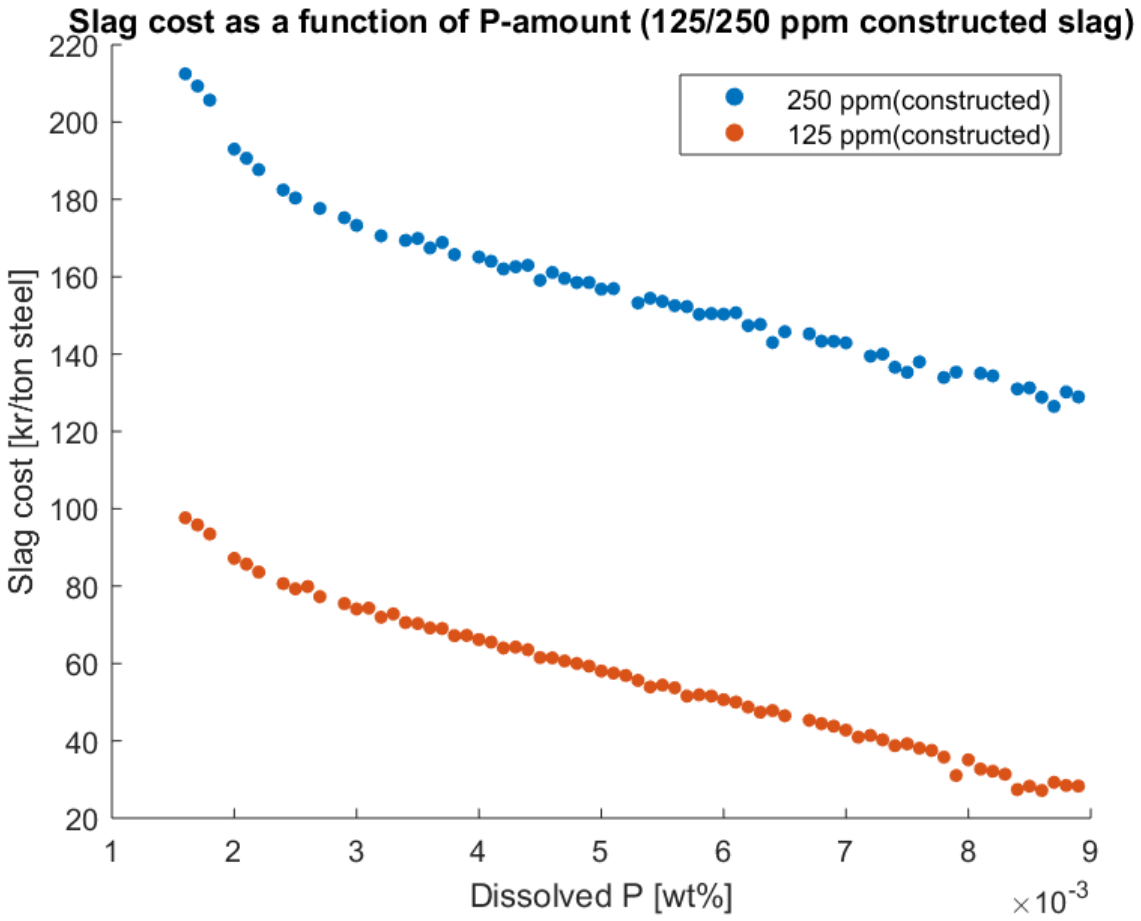

Figure 4.11 Weight optimized slag cost [kr/ton] for different slag compositions as a function of dissolved phosphorus at two initial phosphorus concentrations 250 ppm and 125 ppm ("constructed" slags)

Adding the DRI-based one-slag praxis construction, marked with red and purple data points, yields **figure 4.12.** The amount required for phosphorus removal in 250 ppm case does not differ significantly as of phosphorus levels above 47 ppm below which an exponential increase in slag weight can be seen. Using the one slag praxis, in 125 ppm case, however, yields much larger slag quantities than the two slag praxis "constructed" way.

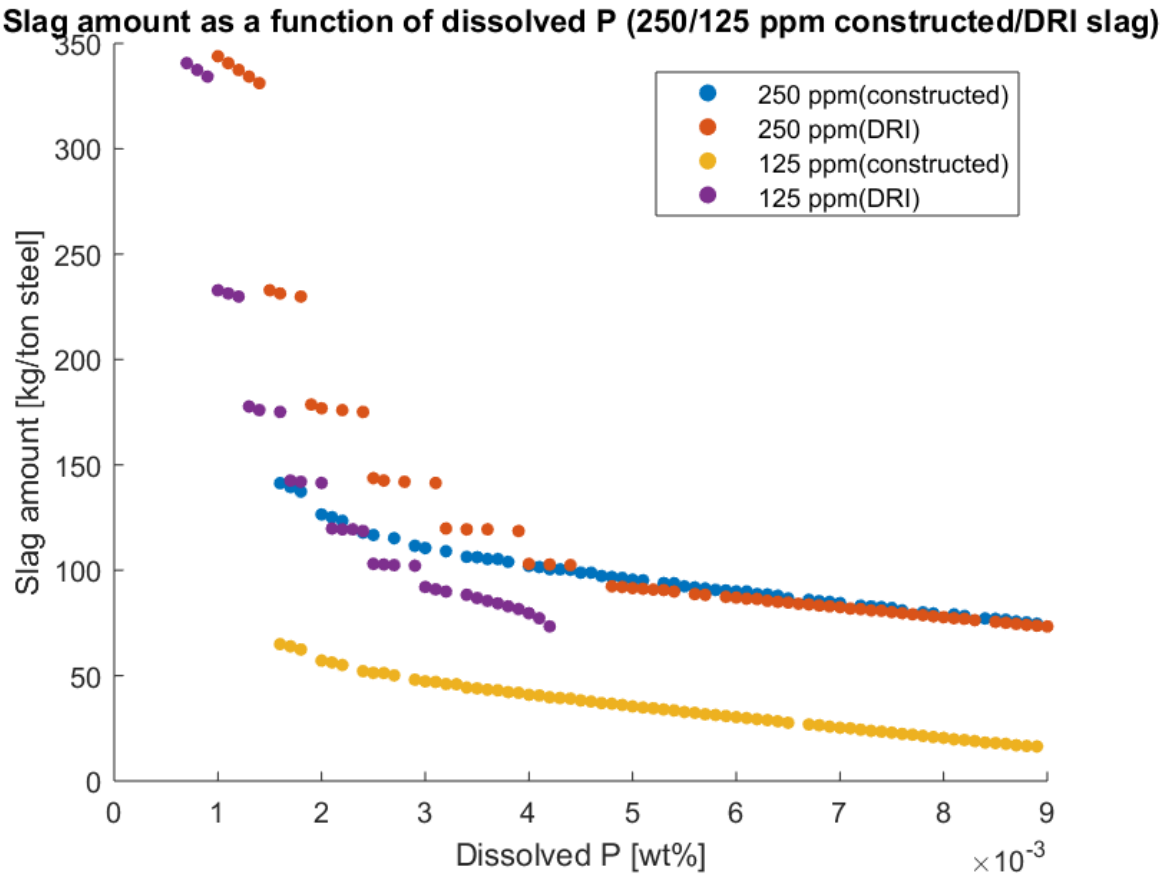

Figure 4.12 Weight optimized slag amount [kg/ton] for different slag compositions as a function of dissolved phosphorus at two initial phosphorus concentrations 250 ppm and 125 ppm ("constructed" and DRI-based slags)

Translated into slag costs, seen in **figure 4.13**, the costs involved with using a one slag praxis for the 250 ppm case is much lower than using a one slag praxis, to a certain point. Below 23 ppm the slag costs rises quickly. However, employing a one slag praxis on the 125 ppm case shows that the two slag praxis can be done at a lesser cost, the yellow data points are always below the purple.

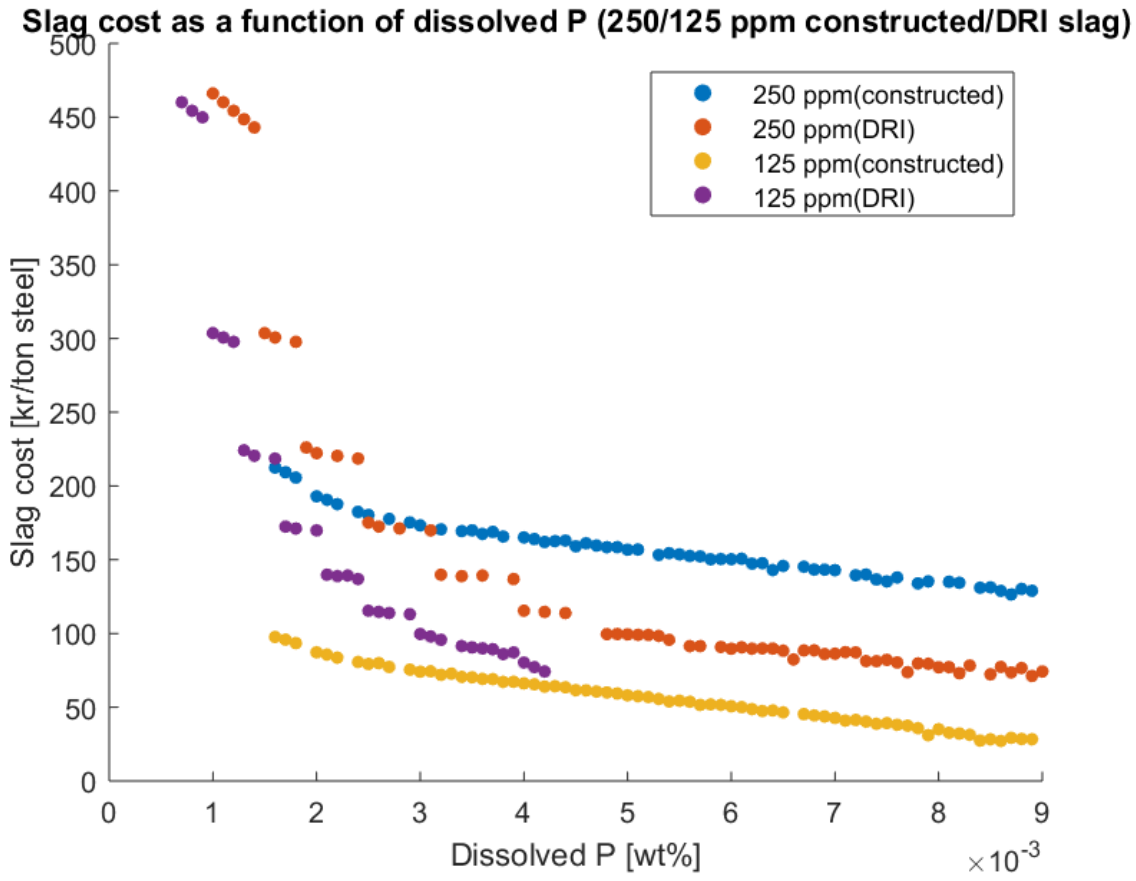

Figure 4.13 Weight optimized slag cost [kr/ton] for different slag compositions as a function of dissolved phosphorus at two initial phosphorus concentrations 250 ppm and 125 ppm ("constructed" and DRI-based slags)

4.3. MgO-saturated slags

The results regarding the three criteria, low phosphorus equilibrium, liquid slag at 1923 **[K]** and MgO-saturation, will be presented below. Out of the 26863 slag compositions created 43 passed the criteria. These compositions vary within a smaller composition range: 48-33 **[wt%]** CaO, 6-12 **[wt%]** MgO, 27-35 **[wt%]** FeO and 15-21 **[wt%]** SiO_2.

The compositions were plotted in a pseudo-ternary phase diagram to visualize the process window for liquid MgO-saturated phosphorus removing slags. The process window can be seen below in **figure 4.14**.

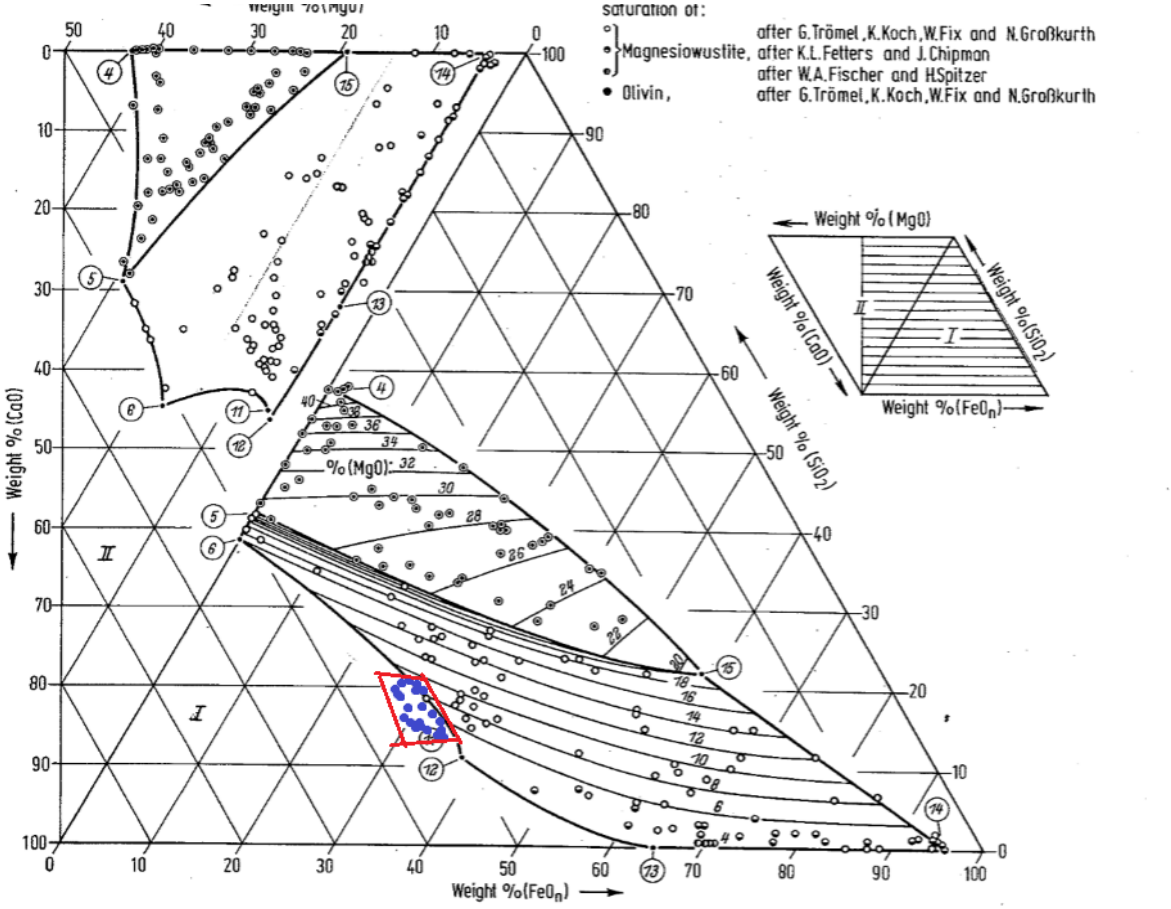

Figure 4.14 Pseudo-ternary phase diagram of the CaO-MgO-FeO-SiO_2 system at 1600°C with passable and optimized slag compositions at 1650°C marked blue and the belonging process window marked with a red square.

5. Discussion

All calculations done in this work are based on thermodynamic equilibrium. Thermodynamic equilibrium never occurs in a real scenario and as such the results presented in this work should only ever be interpreted as trends and the absolute values should never be looked upon and held as true.

5.1. Oxygen and phosphorus calculations

In this study the activity of FeO in the slag controls the oxygen potential in the steel bath and as previously stated, this means that the Gibb's energy functions seen in **equations 3.1** to **3.4** are controlling and become crucial as they are fundamental for all subsequent calculations. The enthalpy as well as the entropy, for the specific Gibb's energy function, has varying values in literature (26) (30) (27). This will influence the oxygen potential in the steel melt. A comparison with "Thermo-Calc" reveals a dissolved oxygen content, at 1923 **[K]** with a FeO-activity of 1, of 0.24 **[wt%]** (32) while the calculations, made in this work, show a dissolved content of 0.1794 **[wt%]**, under the same conditions, **figure 4.2**. While in same order of magnitude these two values differ with 25% which has implications for the dissolved phosphorus content in the steel. The concentration will be higher than in comparable "Thermo-Calc" calculations as high oxygen potential favours phosphorus removal, see **equation 2.9**. The phosphorus amount calculated in this work could therefore, be regarded as conservative, should the "Thermo-Calc" calculations be closer to the truth, even if differences in dissolved oxygen, at high concentrations, i.e. **[wt%]** O > 0.16, does not result in a significant decrease in phosphorus content, at constant P_2O_5-activity, see **figure 4.4**.

Similarly to FeO, data regarding Gibb's energy functions for P_2O_5 varies greatly in literature as $P_2O_5(l)$ is a metastable phase with many allotropic configurations (20). This work is based on a relatively new study in the hope that it provides more accurate data.

5.2. Slag evaluation

One of the requirements imposed was that the slag should provide the conditions for a low phosphorus equilibrium, defined as 0.09 **[wt%]** dissolved phosphorus in the steel. As this study is based on conservative phosphorus calculations fewer slag compositions will pass the phosphorus requirement. The range of passable P_2O_5 interaction coefficients will, therefore, be shifted to the lower range of the spectrum in order to meet the phosphorus criterion. Slags with higher concentrations of CaO are slags that provide a lower P_2O_5 interaction coefficient than more evenly disposed slags. Therefore, along with the shift of the interaction coefficient to the lower range follows a shift in passable slag compositions to the lower range of MgO-concentrations. This should strongly affect the number of passable slag compositions that are saturated in MgO as these compositions, naturally, are relatively high in MgO. Furthermore, the SLAG4 database evaluates solid phases as pure

(32). To find whether a slag is saturated in MgO or not, information was extracted on the phase fractions. If the phase fraction of solid MgO was above 0 the slag was considered saturated. The activity required to nucleate a pure phase is higher than for solid solutions and a slag with high MgO activity is a slag with a high MgO-concentration, roughly speaking. This culminates in that the passable range of MgO-concentrations is pinched from both sides. It should have a higher MgO-concentration due to the way solid precipitates are calculated, and therefore how the saturation requirement is evaluated, and the slag should have a lower MgO-concentration due to the way phosphorus content was calculated. This could provide some insight into why the number of passable MgO-saturated slags is so low in comparison to the number of unsaturated slags, 43 compared to 1564. Calculations without these conflicting biases could reveal a wider composition range for MgO-saturated slags especially, but also a wider range of unsaturated slags. The shift in the MgO-range has further implications as the construction of slags will behave differently.

5.3. Slag construction

Slag compositions with low MgO-content proved to be more difficult to construct, due to a mathematical phenomenon that occurs, that the author calls "self-dilution of slag formers", as a result of impure slag formers. The calcium oxide source, in this case burnt lime, holds 2 **[wt%]** of MgO. As the target composition, of compositions rich in CaO, approached 2 **[wt%]** MgO, the slag weight approaches infinity. This asymptotic behaviour directly corresponds to the MgO-concentration in burnt lime as a slag constructed with mostly a slag former containing 2 **[wt%]** cannot obtain a lower MgO-concentration than that. In some cases, however, MgO-concentrations lower than 2 **[wt%]** could be reached. This is largely due to the pure theoretical slag formers that come into play when slag compositions are more evenly disposed. Nevertheless, the manner in which "self-dilution of slag formers" affects the construction of slags, coupled with the shift in MgO-concentrations discussed above, influences the slag weight required for phosphorus removal, for ultralow concentrations, negatively. The entails that the exponential increase in slag weight as a function of dissolved phosphorus, seen in **figures 4.9**,**4.10** and **4.12**, might be an artefact of the calculations themselves. On the other hand, that lower phosphorus concentrations requires more slag is, when looking at it from a mass balance perspective, intuitively true and that a non-linear proportionality is to be expected can be seen when observing **figure 5.1**, where dissolved phosphorus content is plotted as a function of P_2O_5-activity.

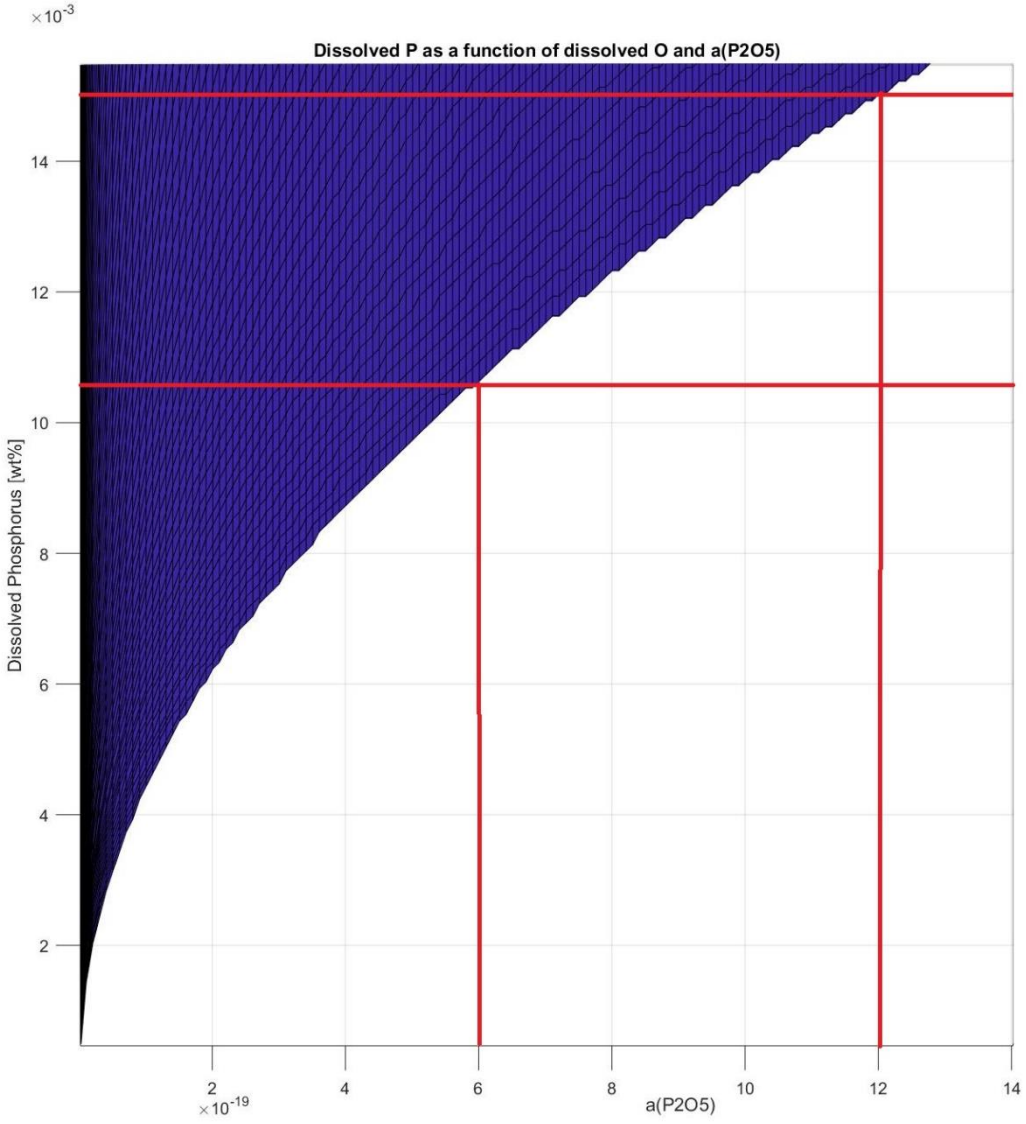

Figure 5.1 Dissolved phosphorus as a function of activity of P_2O_5 at iso- oxygen potential

A doubling of slag weight halves the activity of P_2O_5 in the slag, roughly speaking. This, however, does not result in a halving of dissolved phosphorus in the steel, this is illustrated by the red lines in **figure 5.1,** where the activity of P_2O_5 is halved from 1.2 e-18 to 0.6 e-18. The dissolved phosphorus concentration is calculated using an equation containing exponents and equations with exponents, naturally, does not behave linearly. The non-linear slag weight trend, that is observed, is therefore expected, but can, however, be mitigated to a near linear relation by continuously lowering the P_2O_5-activity coefficient depending on target phosphorus concentration, although in order to do so a new calcium oxide source not containing MgO should be developed, so that self-dilution is circumvented.

5.4. Impact of initial phosphorus concentration

Slag weight is strongly affected by the initial concentration of phosphorus in the raw material. In **figure 4.7** two parallel lines can be seen. The offset of 55 **[kg]**, comparing blue with red trend lines, is strictly due to the initial phosphorus concentration as these compositions are constructed with pure slag formers. When constructed with real slag formers this difference is still to be seen, see **figure 4.10**. Interestingly, lower initial concentrations of phosphorus make the system less susceptible to the effect of self-dilution of slag formers as the exponential increase at low phosphorus concentrations is flatter for the 125 ppm case compared to the 250 ppm case. Furthermore, slag cost and slag weight share a strong correlation which can be observed by examining **figures 4.10** and **4.11**. The slightly more erratic behaviour in **figure 4.11** is a product of the pricing of the different slag formers -some compositions are cheaper to produce from a slag addition perspective. However, higher levels of initial phosphorus concentrations demand a larger slag amount, from a larger slag amount follows higher slag costs and as such removing more phosphorus costs more money. It would, therefore, be recommended for a DRI-based EAF-process to acquire as pure raw material as possible. On the other hand, as stated earlier, a DR-grade pellet is more expensive because of the demand for a purer raw material. Combining knowledge from the pellet producer and the steelmaker is thus crucial as one needs to understand both worlds in order to find an optimum where pureness, and therefore cost, of raw material meets slag amount requirements. The DR-grade premium must not exceed the slag cost savings.

Not only does cost vary with the initial phosphorus amount in the raw material but also praxis that should be used. In **figure 4.12** the DRI-based construction way has been added. The slag amount for the 250 ppm case does not differ significantly until concentrations below 47 ppm. However, the DRI-based construction is a one slag praxis meaning that the slag produced by the melting of pellets is not removed. This provides a “free” source of slag that can be mixed with additional slag formers to reach a target slag composition. As the same amount of slag, for both construction ways, is needed, with the one slag praxis DRI-based way being partially “free”, the DRI-based way should, therefore, yield a lower slag cost. This can also be seen in **figure 4.13**, where the one slag praxis (red line) can be done at a lower cost than the corresponding two slag praxis (blue line). For raw material with a high initial concentration of phosphorus it is, therefore, recommended to employ a one slag praxis. The opposite can be said for raw materials with low initial concentrations of dissolved phosphorus. Here the benefit of a partially “free” slag does not outweigh the cost involved with heating a larger slag amount. The additional costs involved with having a two slag praxis, such as increased tap-tap time, has not been investigated in this study. Some overlap in the cost curves is to be expected as these additional costs are added to the calculations. The difference in construction cost is simply stated, not significant

enough, to make the same conclusion as for the high initial phosphorus content. Further studies aimed at investigating the cost involved with a DRI-based EAF two-slag praxis should, therefore, be conducted.

5.5. MgO-saturated slags

As discussed above only a small number of MgO-saturated compositions passed the criteria. This makes graphical representation similar to those the MgO-unsaturated slags were presented in, difficult, as only a handful of "dots" would be seen spread out on a white sheet. However, graphical representation in a phase diagram is made easier. In **figure 4.14** the optimized compositions that passed the criteria are ordered within a small composition range. Even tough, this process window is located outside the liquidus surface of the phase diagram the condition of a liquid slag is upheld. The phase diagram was a made at 1600°C while the calculations were made at 1650°C. At a higher temperature the liquidus surface will be larger, than at lower temperatures, so that the compositions plotted will be enveloped. The phase diagram, therefore, strengthens the calculations made. To further ensure that the phase diagram and the calculations agree, another set of calculations were made at 1600°C and the corresponding diagram can be seen in **figure 5.2**.

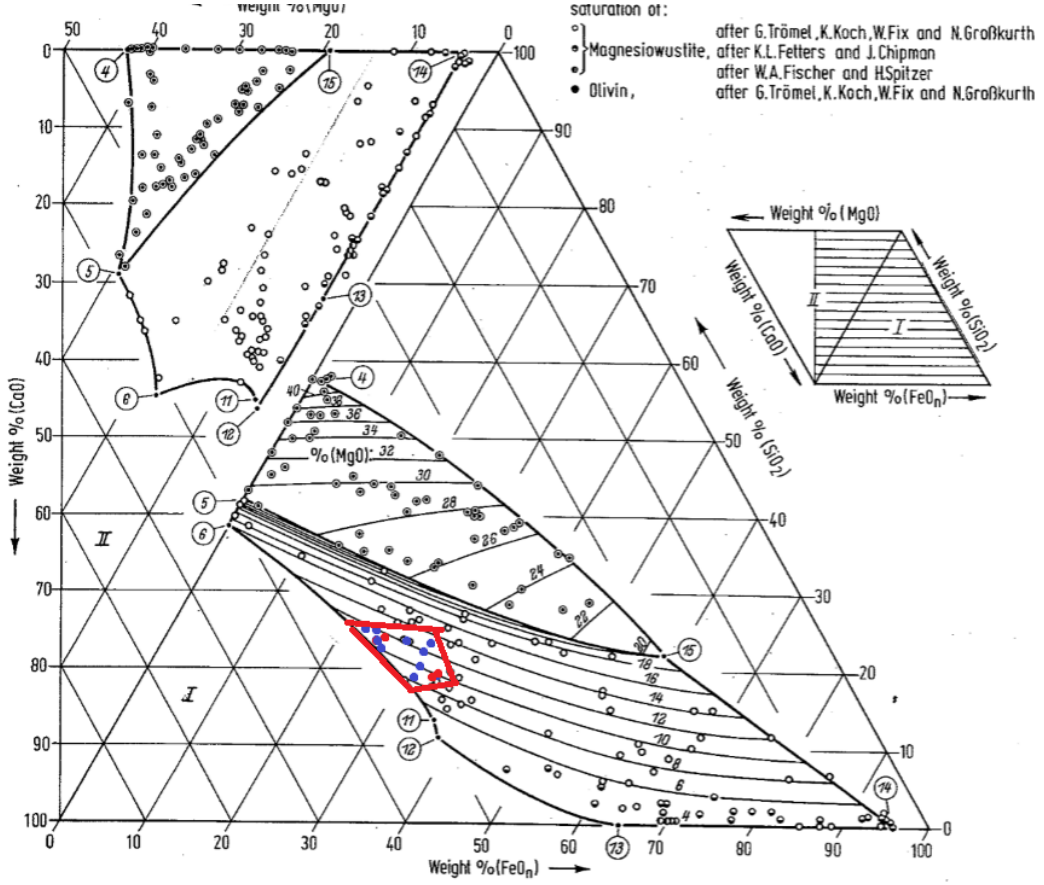

Figure 5.2: Pseudo binary phase diagram of the CaO-MgO-FeO-SiO_2 system at 1600°C with passable and optimized slag compositions at 1600°C marked blue and the belonging process window marked with a red square.

By making a qualitative comparison between the process window in **figure 4.14** and the foaming properties in **figure 2.4** it can be seen that they coincide. These MgO-saturated slags are therefore favourable not only from a refractory protection perspective but also, from the foaming properties that they provide. The process window should, however, be used with care. It has not been investigated whether all the compositions defined within the process window allow for efficient phosphorus removal as the combination of P_2O_5-interaction parameter along with the FeO-activity that the compositions, within this window, provide has not been verified, by this study, to be adequate.

6. Conclusions

A tool for optimising the slag system in a DRI-based EAF-process has been developed. Using 17 modules programmed in "Matlab" 26863 slag compositions were created in a bias-free environment and then evaluated. The P_2O_5-interaction parameter, calculated using Somnath Basu's empirical model, and the activity of FeO, calculated using "Thermo-Calc" (33), provided the basis for how capable the different compositions were at removing phosphorus. Restrictions such as a liquid slag, maximum allowed phosphorus equilibrium content and MgO-saturation were then imposed. The compositions that passed the criteria were thereafter optimized after slag weight.

In this study it was found that:

- Slag weight correlated well with slag cost as well as phosphorus concentration linking slag cost to the initial phosphorus concentration in the raw material.
- Low initial phosphorus concentrations were deemed preferable from an economic standpoint although further collaboration between a pellet producer and a steelmaker is required to find the optimal initial phosphorus concentration.
- Preferable slag praxis was dependent on initial phosphorus concentration in the raw material. For low initial concentrations a two slag praxis should be further investigated and for a high initial concentration a one slag praxis should be employed in order to minimize slag costs.
- MgO was found to be a problem for slag cost optimization as the burnt lime slag former contained low amounts MgO. This resulted in higher slag weights than could be achieved due to a mathematical difficulty that arises when constructing slags, that the author has chosen to describe as "self-dilution of slag formers".
- A MgO-free calcium oxide slag former should be developed for ultralow phosphorus steels.

- A process window was established when 43 MgO-saturated compositions, that passed the set of criteria, were found. These compositions show promise not only based on the refractory protection they provide but also based on their potential foaming properties. This process window should, however, be used with care.

6.1. Epilogue

This work is a but small step of progress in the grand scheme of things. Although, just as any 10.000-mile journey begins with a single stride so too must the steel industry be revolutionized, step by step, to help ensure our planets continued survival.

7. Acknowledgements

I would like extend my sincerest appreciation to my supervisors Dr. Niklas Kojola at SSAB AB, Research and Innovation, and Prof. Pär Jönsson as well as to my mentors Prof. Du Sichen and PhD-student Martin Berg at the Dept. of Material Science and Engineering at KTH, for their never wavering patience when faced with the questions of lesser men.

8. References

1. **Nyman, Anna-Karin. Så ska stålindustrin bli fossilfri** jernkontoret.se. [Online] Jernkontoret, den 4 April 2016. [Citat: den 7 May 2018.] https://www.jernkontoret.se/sv/publicerat/nytt-fran-jernkontoret/nyheter/2016/nytt160404_vatgasprojekt/.

2. **Karsberg, Viktoria. SSAB,LKAB och Vattenfall tar initiativ till en koldioxid-fri stålindustri** ssab.se. [Online] SSAB, den 4 4 2016. [Citat: den 7 May 2018.] https://www.ssab.se/GlobalData/News-Center/2016/04/04/05/32/SSAB-LKAB-och-Vattenfall-tar-initiativ-till-en-koldioxidfri-stlindustri.

3. **Jernkontoret. HYBRIT- Fossilfri stålproduktion** jernkontoret.se. [Online] Jernkontoret, den 1 February 2018. [Citat: den 7 May 2018.] https://www.jernkontoret.se/sv/vision-2050/koldioxidfri-stalproduktion/.

4. *CO2 EMISSIONS IN THE STEEL INDUSTRY.* **KUNDAK, M., LAZIC, L. och CRNKO, J.** 3, u.o. : METALURGIJA, 2009, Vol. 48.

5. **HYBRIT.** Hybrit Brochure. *Summary of findings from HYBRIT Pre-Feasibility Study 2016-2017.* u.o. : HYBRIT, 2018.

6. **SESHADRI, SEETHARAMAN.** *Treatise on Process Metallurgy Industrial Processes, Part A.* u.o. : Elsevier, 2013.

7. **Yuhas, Alan. Dagger in Tutankhamun's tomb was made with iron...** theguardian.com. [Online] The Guardian, den 2 June 2016. [Citat: den 7 May 2018.] https://www.theguardian.com/world/2016/jun/01/dagger-king-tut-tomb-iron-meteorite-egypt-mummy.

8. **Andersson, Margareta och Sjökvist, Thobias.** *Processmetallurgins Grunder.* Stockholm : Kungliga Tekniska Högskolan, 2002.

9. **Hannah, Peter. Iron ore price trends and assessing DR-Grade Pellet Premium** metalbulletin.com. [Online] den 25 April 2016. [Citat: den 10 05 2018.] http://www.metalbulletin.com/events/download.ashx/document/speaker/8882/a0ID000000ZxkH2MAJ/Presentation.

10. **Regeringskansliet Miljö- och energidepartementet. Målet är ett Fossilfritt Sverige**. *http://www.regeringen.se/4add1a/contentassets/790b8b0d7c164279a39c9718ae54c025/faktablad_fossilfritt_sverige_webb.pdf.* u.o. : Regeringen, 2015.

11. **TREMAG. Electric Arc Furnace picture** [Online] [Citat: den 24 05 2018.] http://tremag.ro/industries/nonferrous-metals-industry/electric-arc-furnace-for-copper-melting/.

12. **ABB. Electric arc furnace picture** abb-conversations.com. [Online] ABB, 10 2013. [Citat: den 24 05 2018.] https://www.abb-conversations.com/2013/10/energy-efficiency-in-steel-is-about-striking-when-and-where-the-iron-is-hot/.

13. **Pretorius, Eugene och Oltmann, Helmut.** *EAF Fundamentals.* [PDF] u.o. : LWB Refractories-Process Technology Group , 2017.

14. *The electric arc furnace process: towards an electricity consumption below 200 kWh/t.* **Scheele, Joachim von.** Stockholm : Scandinavian Journal of Metallurgy, 1999, Vol. 28. 0371-0459.

15. *Electromagnetism and the Arc Efficiency of Electric Arc Steel Melting Furnaces.* **et.al, A. N. Makrov.** Tver : Journal of Electromagnetic Analysis and Applications, 2014, Vol. 6.

16. **American Metal Market.** *Sparks fly in graphite electrode market.* [PDF] u.o. : American Metal Market, Oct 2017.

17. *Stabilization of soils with steel slag and cement for application in rural and low traffic roads.* **Barra, M.** Arlington : Proceedings of the Beneficial Use of Recycled Materials in Transportation Application, 2001.

18. *Characteristics of the slags produced in the fusion of scrap steel by electric arc furnace.* **Luxán, M. P.** 4, u.o. : Cement and Concrete Research, 2000, Vol. 30.

19. *Durability of concrete made with EAF slag as aggregate.* **Manso, J. M.** 6, u.o. : Cement and Concrete Composites, 2006, Vol. 28.

20. *Thermodynamic Assessment of P2O5.* **Hudon, Pierre.** 11, u.o. : Journal of the American Ceramic Society, 2012, Vol. 95.

21. *On the Phosphorus Partition between Liquid Steel and BOF Slag .* **Basu, Somnath.** u.o. : ISIJ International, 2007.

22. **Verein Deutscher Eisenhüttenleute (VDEh).** *Slag Atlas.* Düsseldorf : Verlag Stahleisen GmbH, 1995. 3-514-00457-9.

23. **(SSAB), Niklas Kojola.** 04 2018.

24. **Vykopal, Jan, Plesnik, Tomas och Minarik, Pavel.** *Network-based Dictionary Attack Detection.* Brno : Masaryk University Institute of Computer Science.

25. **Mathworks. Matlab**. *Mathworks.* [Online] Mathworks. [Citat: den 31 05 2018.] https://se.mathworks.com/products/matlab.html.

26. *A thermodynamic assessment of the iron-oxygen system.* **P.J. Spencer, O. Kubaschewski.** 2, u.o. : Calpjad, 1978, Vol. 2.

27. **Knacke, O., Kubaschewski, O. och K.Hesselmann.** *Thermochemical Properties of Inorganic Substances Second edition .* Aachen : Springer-Verlag; Verlag Stahleisen, 1991. 3-540-54014-8.

28. **Hayes, Peter.** *Process Principles in Minerals and Materials Production.* Brisbane : Hayes Publishing CO, 1993. 0-9589197-3-9.

29. *Thermodynamic Assessment of P2O5.* **Jung, In-Ho och Hudon, Pierre.** 11, Montre´al : The American Ceramic Society, 2012, Vol. 95.

30. **Turkdogan, E.T.** *Physical Chemistry of high temperature technology.* New York : Academic Press, 1980. 0-12-704650-X.

31. **Gaskell, David R.** *Introduction to the Thermodynamics of Materials.* New York : Taylor & Francis Group, 2008. 1-5916-9043-9.

32. **Thermo-Calc.** *TCFE Steels/Fe-alloys database version 9 (accessed 05 Mai 2018).* u.o. : Thermo-Calc.

33. —. *Thermo-Calc Software SLAG TCS Fe-containing Slag Database version 4 (accessed 05 Mai 2018).* u.o. : Thermo-Calc.

34. **MetalBulletin.** *Iron Ore Index- Daily Market Report.* u.o. : MetalBulletin, 19 feb 2018.

35. **Investing.com.** ***Investing.*** **[Online] [Citat: den 05 03 2018.] https://www.investing.com/currencies/usd-sek.**

36. ***An overview of utilization of slag and sludge from steel industries.*** **et.al, B. Das. 40-57, u.o. : Resources, Conservation and Recycling, 2007, Vol. 50.**